NEUTRON CAPTURE CROSS SECTIONS

IN THE KEV REGION

by

Lawrence Wilson Weston

Department of Physics
Duke University

Date: April 18, 1960

Approved:

Henry W. Newson
Henry W. Newson, Supervisor

Eugene Greuling

H. W. Lewis

H. Staner.

J. D. Dessel

A dissertation submitted in partial fulfillment of the requirements for the degree of Doctor of Philosophy in the Department of Physics in the Graduate School of Arts and Sciences of Duke University

1960

ACKNOWLEDGEMENTS

I would like to express my sincere appreciation to Dr. H. W. Newson who suggested these experiments and rendered invaluable help in every phase of the preparation of this dissertation. I especially wish to thank Dr. E. G. Bilpuch for his many long hours of assistance with experimental details, and interpretation of the data. I also extend thanks to the entire Van de Graaff group for their help in taking the data, and to Dr. K. K. Seth for his advice on the analysis of the average total cross section data, and his programing of the optical model calculations for use at the Computation Center at Duke University. The provision of absolute capture cross section measurements prior to publication by groups at Oak Ridge National Laboratory, Los Alamos and the Lawrence Radiation Laboratory was of great value.

This work was supported by the United States Atomic Energy Commission.

L. W. W.

CONTENTS

	Page
Introduction	2
Chapter	
I. EXPERIMENTAL PROCEDURE	6
Technique of Measurements	6
Neutron Monitors	11
Background Corrections	16
II. METHOD OF ANALYSIS	19
III. INTERPRETATION OF EXPERIMENTAL RESULTS	35
IV. P-WAVE STRENGTH FUNCTIONS	52
APPENDIX	
I. AVERAGE TARGET THICKNESS	63
II. HYDROGEN RECOIL COUNTER	78
REFERENCES	89

LIST OF FIGURES AND TABLES

Figure — Page

1. Reaction Cross Section of B^{10} 12
2. Normalized Ratio of BF_3 and McKibben Counting Rates. 14
3. Capture Cross Section of U^{238} 25
4. General s-Wave Contribution For I = 1/2 Target Nucleus 30
5. Capture Cross Section of Mo^{100} 37
6. Capture Cross Section of Ag^{107} 38
7. Capture Cross Section of Ag^{109} 40
8. Capture Cross Section of In^{115} 41
9. Capture Cross Section of I^{127} 43
10. Capture Cross Section of As^{75} 44
11. Capture Cross Section of Rh^{103} 46
12. Capture Cross Section of Pd^{108} 47
13. Capture Cross Section of Au^{197} 49
14. Capture Cross Section of Pt^{198} 51
15. p-Wave Strength Functions. 53
16. Thick Target Threshold 68
17. Forward Threshold For a 1.6 kev LiF Target 71
18. Neutron Back Threshold at 90° with BF^3 Counter . . . 77
19. Hydrogen Recoil Counter. 79
20. Differential Recoil Spectrum of 200 kev Neutrons . . 82

Tables

I. McKibben Counter Efficiency Versus Neutron Energy. . 15

II. Summary of Parameters. 58

NEUTRON CAPTURE CROSS SECTIONS

IN THE KEV REGION

INTRODUCTION

The neutron capture cross section $\sigma_{n\gamma}$ as a function of energy may be measured most readily in the lower kev region by means of the β-radiation which frequently follows capture. This method has been used extensively both for the detection of individual resonances in light or magic nuclei[1] and for the measurement of capture cross sections averaged over many resonances for normal heavy nuclei.[2] The most interesting region for the latter experiments lies between about three and one hundred kev where, in most cases, only s- and p-wave neutrons contribute appreciably to the capture cross sections. Because of increasing difficulty in correcting for background and in maintaining a neutron energy spread much less than the average neutron energy (when it is less than about three kev), an activation technique with (relatively) homogeneous neutron beams cannot usually be extended to energies low enough that only s-wave neutrons are captured. However, there is now enough information on s-wave parameters to allow us to subtract off the s-wave contribution and to determine p-wave capture cross sections to a useful approximation in many cases.

The importance of neutron absorption cross sections in the ev and thermal energy region is primarily due to their usefulness in nucleonics; however, in the kev region of neutron energy they provide an important means of studying the interactions of neutrons of different angular momenta with respect to the nucleus.[3] Up to the neutron energy of a hundred kev only s-, p-, and to a slight extent, d-wave neutrons contribute to neutron cross sections, and one may expect to analyze the data for these separate components. At higher energies such an analysis is much more difficult because of the participation of a large number of inelastic levels and angular momenta. Thus absorption cross sections in the energy region of one to one hundred kev are particularly interesting.

The optical model of the nucleus was initially proposed by Feshbach, Porter and Weisskopf[3] for neutrons, and received remarkable support from neutron total cross section data of Barschall et al.[4] However, while giant resonances, due to different angular momenta, were observed in total cross sections, finer effects such as spin-orbit coupling could not be detected in this data. The reason for this discrepancy is simple. The major part of neutron total cross sections above a few kev is nearly always due to s-wave potential scattering and smaller effects superimposed on it are difficult to detect.[5] Neutron capture cross sections, on the other hand do not suffer from this disadvantage since there is no "potential" capture. In addition, penetration factors inhibit the capture of p-wave neutrons to a much smaller extent than for scattering. The present series of

experiments were designed to exploit these advantages.

The optical model predicted resonances in the p-wave neutron strength function in the neighborhood of A = 28, 90 and 216. These are all indicated in the total cross section data of Barschall et al.[4] However, only preliminary investigations of p-wave neutron strength functions (such as those made for s-wave resonance parameters in the neighborhood of A = 50[6-9] and 140[10] have so far been made.[11,12]

Unfortunately in the region of atomic weight with which this study is concerned, it is nearly always impossible, with present experimental techniques, to resolve individual resonances in the kev region sufficiently well to use the method of individual resonance analysis for p-wave neutrons. However, in our region of atomic weight where the p-wave cross section is high, it is possible to analyze averaged total cross section data for p-wave neutron strength functions.[11]

An intensive study of average neutron capture cross sections of nuclei with $75 \leq A \leq 130$ has been carried out in the neutron energy region of three to two hundred kev, using the activation method. Assuming s-wave parameters within the limits of error specified by low-energy total cross sections determinations, the data has been analyzed for corresponding p-wave parameters; the neutron strength function, $\overline{\Gamma}_n^{(l)}/D$, and the γ-ray strength function, $\overline{\Gamma}_\gamma/D_o$. It is found that the s- and p-wave γ-ray strength functions are the same within the rather large limits of experimental error for the odd A targets: As^{75}, Rh^{103}, Ag^{107}, Ag^{109}, In^{115}, I^{127}, Au^{198}. The even-even isotopes of Pd, Mo, Pt, and U

are more complicated in this respect.

P-wave neutron strength functions, $\overline{\Gamma}_n^{(1)}/D$, derived from the analysis of these capture cross sections are found to be in agreement with $\overline{\Gamma}_n^{(1)}/D$ as obtained from the analysis of neutron total cross sections. These strength functions exhibit a broad, double peaked, distribution around A = 100 instead of the single peak predicted by the simple optical model. It is shown that the experimental results may be explained by the addition of a small spin-orbit part to the optical potential. The parameters of the square well optical potential $V^{\pm} = V_o \left[1 + i\xi + \delta/2 \{-1 \pm (2\ell + 1)\}\right]$ which are found to fit the p-wave strength functions best are V_o = 41 Mev, ξ = 0.02, δ = 0.085, and $R = 1.45\ A^{1/3}$ fermis.

Chapter I

EXPERIMENTAL PROCEDURE

Technique of Measurements

Protons, produced by the four Mev Duke Van de Graaff accelerator, were first sent through a magnetic deflection system then through an electrostatic analyzer. The beam at the target was usually between four and ten micro-amperes. The proton energy spread was about 1/1500 of the proton energy. A thin lithium or lithium fluoride target (stopping power about 2 kev) was evaporated on a disc of 0.002-inch platinum after the disc had been soldered across the end of a 3/4-inch silver tube. The tube wall thickness was 0.010 inch; the neutron transmission ratio for this thickness is greater than 99.5 percent. A ring-shaped sample to be bombarded by neutrons was placed in a cadmium holder around the silver tube normal to the direction of the proton beam, and co-planar with the target. Consequently, all the neutrons that left the lithium target in a small polar angle about 90° were intercepted by the sample.

The energy spread of the neutron beam which the ring-shaped sample intercepted was determined almost completely by the target thickness and the finite angle subtended by the sample; target thickness effects are important only at the lower energies (< 25 kev). The average neutron energy and its energy spread at 90° from the target were determined both by forward threshold analysis (see Appendix I), and by the less accurate method of observing the shape of the 90° threshold as measured by a small BF_3 counter. The average proton energy was taken to be the mid-point of the energy spread due to the target thickness and the proton energy spread. The neutron energy spread (ΔE_n) was $\pm$ 1 kev at 3 kev, $\pm$ 5 kev at 10 kev, and $\pm$ 10 kev at 100 kev, including the effects of the width of the ring-shaped samples (0.10 inch), the target thickness, and the energy spread of the proton beam. Since the average target thickness was the least well known factor in the resolution, the targets were carefully picked so they would not cause the major spread in the energy in any region under study. For practical purposes the targets used below E_n = 15 kev were less than E_p = 2 kev thick.

As can be seen from the discussion above, the resolution ($\Delta E_n/E_n$) was not very good in the energy region from three kev to fifteen kev. The effect of the poor resolution in this range upon the experimental data was less than would be suspected at first sight. The angular acceptance of the sample was the main contributor to the neutron energy spread. The neutron energy variation with angle was due principally to the center of mass motion of the Li(p,n) reaction. A simple geometrical calculation

shows that around 90° with respect to the proton beam the neutron flux per neutron energy interval (number of neutrons/ΔE_n) is approximately a constant even though the angular distribution of the neutron intensity is a rapidly changing function with angle. Thus our energy distribution about the nominal energy was roughly rectangular. A precisely rectangular shape would imply that our average capture cross section measurements were a true algebraic mean. The fact that the neutron monitor used in this energy region (BF_3 counter) had an $E_n^{-1/2}$ energy dependance (roughly the same shape as the capture cross sections) further reduced any distortion of the average cross section curve which might arise from the rather large values of $\Delta E/E$ below fifteen kev.

In order to measure the average capture cross section it is necessary that the average resonance spacing be much less than $2\Delta E_n$ so that the capture at each nominal neutron energy is due to many resonances. This is true for most normal heavy elements, i.e., those not too close to a neutron magic number. However, the same experimental technique can be used to locate well separated resonances in light or magic nuclei[1] when the spacing, $D \gg 2\Delta E_n$.

Since there was a continuous generation of radioactive nuclei during an exposure, a correction was made for those nuclei which had decayed during the exposure. This was done by recording a neutron monitor counting rate at intervals which were short compared to the half-life activated. The count C_i in every time interval was then multiplied by the appropriate value of $e^{-\lambda t_i}$ where λ is the decay constant and t_i was the time from

the i^{th} interval to the end of the exposure. The sum $\sum_1(C_i\ e^{-\lambda t_i})$ then gave the monitor count which would have been recorded if all radioactive nuclei had been formed instantaneously.

The induced activity was measured with a thin wall beta counter, and the decay was followed for several half-lives to insure the identification of the radioactive nuclide. The initial beta yields from the samples were at least three times the beta counter background, and no problem was encountered in making this background correction. These yields remained approximately constant as a function of energy because, as the capture cross section decreased with energy, the neutron yield at 90^{o} increased. Each sample was handled in exactly the same manner.

Of the eleven nuclides for which capture cross sections were measured, the following were activated in the form of thin ribbons of the naturally occurring metals wrapped around the Li target holder; the dimensions (in inches) follow: Mo^{100}(0.002 x 0.10 x 8), Rh^{103}, $Ag^{107,109}$, Pd^{108}, Au^{197}, and Pt^{198} (each 0.001 x 0.1 x 12.0) and In^{115} (0.001 x 0.1 x 2.5). Arsenic, Uranium Oxide (U^{238}), and Potassium Iodide (I^{127}) were pressed in the form of rings 7/8 inch internal diameter, 1/10 inch in length and 1/16 inch in thickness. The KI sample could be conveniently used since the K^{40} natural activity background was very much lower than I^{128} activity being measured. The activation measurements on U^{238} were not done by the author. A complete description of the experiment, including the method of separating the radioactive daughter products from Uranium, may be found in the Ph.D. dissertation of Dr. Edward G. Bilpuch.[13]

For Ag^{107}, Ag^{109} a separate experiment was made using a Geiger counter made out of thin walled silver tubing three inches long and 1/4 inch in diameter. This Geiger tube was placed near the target so as to subtend the same polar angle as the foil samples and acted both as the sample being activated and the counter for the induced activity. It was connected to an automatic recording scaler which followed the β-decay (after the beam was cut off), without having to disturb the counter. The most reliable data on the rather short (24 second) half life activity of Ag^{110} was obtained in this way; the results of this experiment for Ag^{107} capture cross sections were in good agreement with those of the foil activation.

In the experiments reported here, only the relative neutron capture cross section as a function of energy was measured since the methods most suitable for detecting activation below 120 kev are unsatisfactory for absolute measurements. The activation technique for measuring capture cross sections is restricted to the fraction of nuclides ($\sim$ 25 percent) which can be activated conveniently. This method has the great advantage that, in general, separated isotopes are not needed; the half-life allows us to assign the induced activity to the proper isotope. For the same reason, chemical compounds can also be used as samples in many cases.

The relative capture cross section curves were normalized to absolute measurements performed in other laboratories. These latter experiments are very difficult, and the agreement between measurements by different methods is still not entirely satis-

factory, but the available data is sufficiently accurate for at least a partial interpretation of our relative capture cross section curves.

Neutron Monitors

In order to measure the true shape of an activation cross section curve it is necessary to measure the relative neutron flux at each activation. This monitoring should depend on a nuclear process of known neutron cross section. We have chosen the neutron-proton scattering[14,15] and the $B^{10}(n,\alpha)$ cross sections as standards since these cross sections can be measured by simple transmission measurements. As a secondary standard we have used a McKibben counter as our neutron monitor.[16] The BF_3 counter used in the McKibben is six inches long with a diameter of one inch and filled to a pressure of 50 cm (Hg) with enriched $B^{10}F_3$.

The total cross section of B^{10} in the region 3 kev to 100 kev was measured by Rohrer[17] with the 122° neutron collimator described by Gibbons.[18] The potential cross section of boron has been measured up to twenty kev and has the value of 2.43 barns.[19] This potential cross section was then subtracted from the total cross section of B^{10}. In this manner we obtained $\sigma(n,\alpha)+(n,\alpha,\gamma)=\sigma_{n\alpha}$ which is equal to $642/\sqrt{E}$ within statistical errors. The results are shown in Figure 1. Similar results in the ev region have been reported by Schmitt <u>et al.</u>[20] Up to seventy kev we find that $\sigma_{n\alpha}$ for B^{10} goes as 1/v where v is

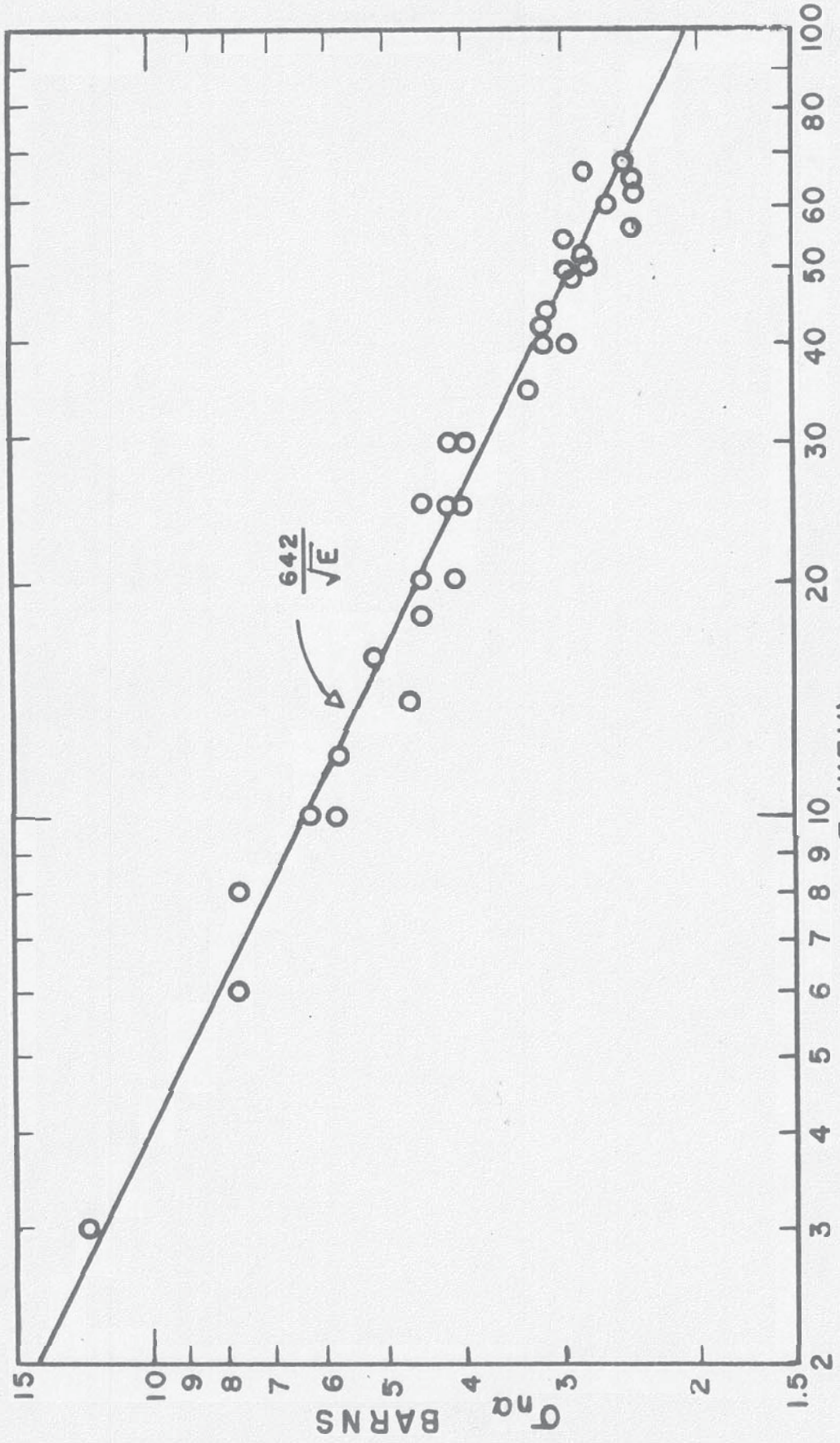
REACTION CROSS SECTION OF BORON 10
$\frac{642}{\sqrt{E}}$
$\sigma_{n\alpha}$ BARNS
E_n(KEV)
15
10
9
8
7
6
5
4
3
2
1.5
2
3
4
5
6
7
8
9
10
20
30
40
50
60
80
100

Figure 1

the neutron velocity. On the basis of the experiments about to be described, we suspect that the scattering cross section increases above seventy kev and that the reaction cross section of B^{10} continues as 1/v beyond one hundred kev. A 1/v dependence for $B^{10}(n,\alpha,\gamma)Li^7$ has also been reported by Gibbons et al.[21]

Since $\sigma_{n\alpha}$ of B^{10} follows the 1/v law at least up to seventy kev the "flatness of response" of the long counter (McKibben) was tested in the following manner. A bare BF_3 counter surrounded by Cd was placed at 90° to the proton beam, and its counting rate was observed as a function of energy. At each corresponding energy and at the same angle, the neutron flux was monitored by the long counter. If the long counter was constant in efficiency then the ratio (BF_3 counting rate)/(long counter rate) at each energy would go as 1/v. The results of this ratio are shown in Figure 2. The experimental points have been normalized to the solid line which is given by $642/E_n^{1/2}$. If we assume that the long counter is constant in efficiency then Figure 2 gives $\sigma_{n\alpha}$ for B^{10} up to three hundred kev. Similar results on the same assumption have been reported by Bichsel and Bonner.[22]

To show that the long counter is constant in efficiency at the higher energies, a hydrogen recoil-counter was constructed. Appendix II gives a detailed description of this recoil counter. At zero degrees the neutron flux was measured from 100 kev to 650 kev neutron energy. At the same angle and energy long counter measurements were taken. These two curves showed the shape of the zero degree differential cross section for the $Li^7(p,n)Be^7$ reaction.[23] For simplicity Table I shows the ratio (long counter)/

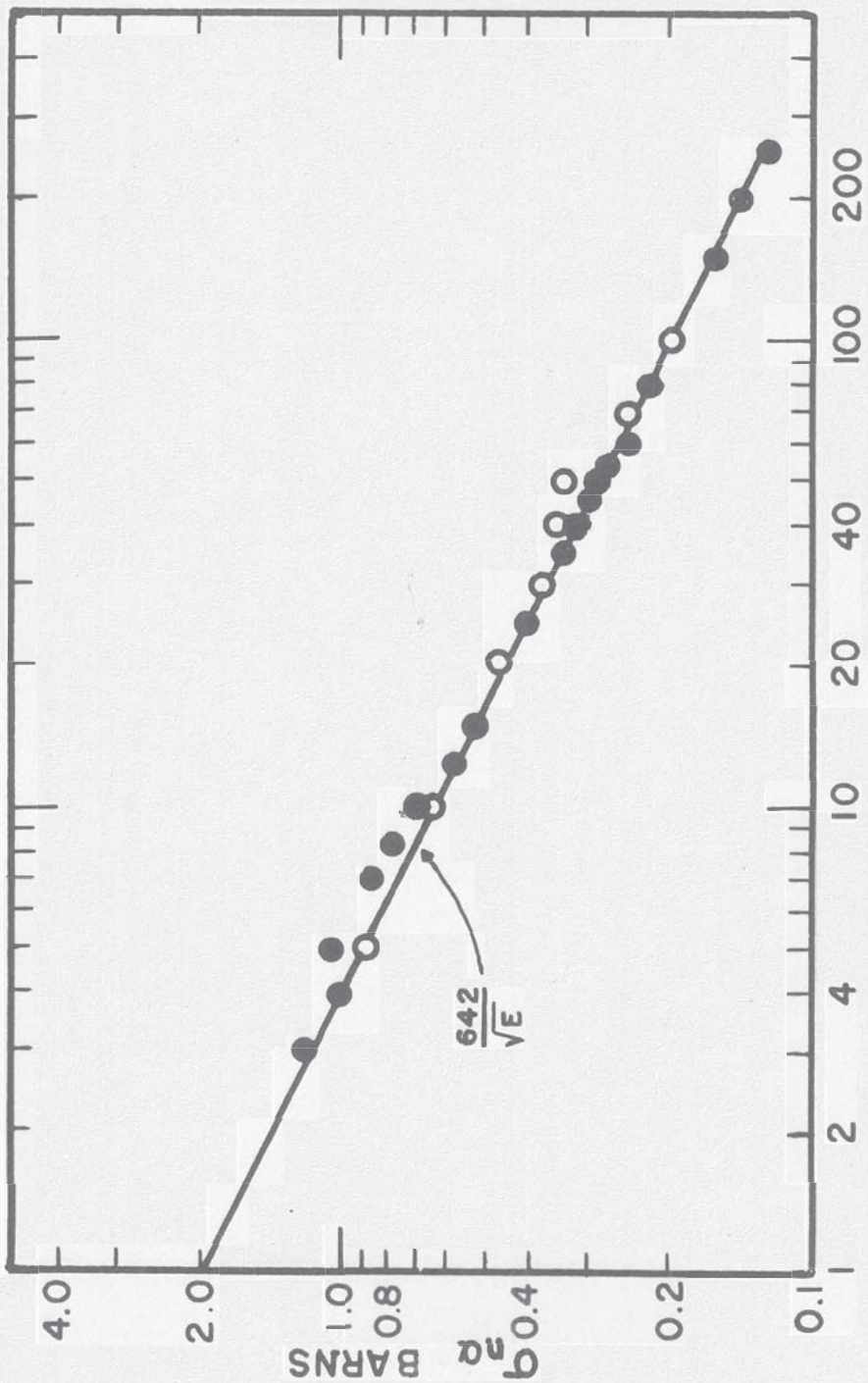

NORMALIZED RATIO OF BF_3 AND MCKIBBEN COUNTING RATES

Figure 2

TABLE I. McKIBBEN COUNTER EFFICIENCY

E_n (kev)	100	150	200	300	400	500	650
McKibben [a] Counts/20μq	14,288	6,968	4,893	2,823	3,491	11,455	11,974
Recoil Counts/20μq	17,800	7,370	4,540	2,180	2,420	7,310	6,970
Integrated Neutron Flux Through Recoil Counter	110,000	53,000	36,300	20,900	26,600	87,000	90,600
Ratio of McKibben Counts and Integrated Flux	0.130	0.132	0.135	0.135	0.131	0.132	0.132
Percent Deviation [b] from Mean	-1.8	-0.4	+2.0	+2.0	-1.1	-0.4	-0.4

(a) The 20μq refers to the integral of the proton charge.

(b) Estimated uncertainties due to recoil counter corrections are ± 3 percent.

(recoil counter). This table shows that this ratio does not vary with energy from 100 to 650 kev. The two experiments described in the preceding paragraphs show that within experimental error our long counter is constant in efficiency in the energy regions 3-70 kev and 100-650 kev and from Figure 2 it appears that this is also true from 70-100 kev.

Background Corrections

Neutrons were scattered toward the sample by the 0.002 inch platinum backing of the target and also by the walls, floor and atmosphere of the laboratory. In order to correct for the effects of these scattered particles, a sample was placed in position, and the proton energy was adjusted so that neutrons from the Li(p,n) reaction were produced at 80° or less from the forward direction. Hence, with the sample at 90°, no direct neutrons could bombard it, so that any observed activation could be due only to scattered neutrons. The activation in this experiment was almost indetectable and amounted to only a few per cent of the 90° neutron beam activation. Except at the lowest neutron energies used in these measurements, where the yield of the 90° neutrons near threshold was very low, the scattered neutrons contributed negligibly to the activation of the sample because most of the neutrons scattered emerge at forward angles in the laboratory system and consequently have higher energies than the 90° neutrons; the latter are captured much more readily since the average absorption cross section in the kev region falls off

as $1/E_n^{1/2}$ or faster. The relatively large solid angle intercepted by a ring-shaped sample about the target was an equally important factor which reduced the relative importance of room scattered neutrons among those causing activation.

The background due to scattered neutrons, although not a problem so far as the activation of the sample was concerned, was very important in the monitoring of the neutron beam. At low neutron energies a small BP^3 counter (2.5 inches long and 0.5 inch in diameter) was used for this purpose. In order to subtend the same polar angle at the target as the sample, the counter had to be placed farther away so that it subtended only about one-sixth as much solid angle as the sample. Hence, the room scattered neutron background became appreciable (although still only about ten percent) and had to be measured with the help of shadow cones. A BF_3 counter is, like the sample, relatively insensitive to the high energy neutrons scattered from the room or the target backing, and for this reason we always prefer to use a bare BF_3 counter as a monitor at least up to twenty kev.

The long counter, when used as a neutron monitor, has a constant efficiency over a wide energy range and will detect scattered and direct 90° neutrons equally well. Therefore, the room scattered background and the target scattered background of this neutron monitor were important corrections. The room background depends on the total yield of the $Li^7(p,n)$ reaction (above back threshold, 1.920 Mev.) and hence is a slowly varying function of proton energy, but up to E_n = 10 kev the 90° neutron yield is rapidly increasing. Consequently, in the region above

about twenty kev, the scattered background is not a very important part of the total flux observed by the long counter so that it is the most satisfactory monitor from about fifty kev to several Mev.

Chapter II

METHOD OF ANALXSIS

It is our purpose to analyze the observed capture cross sections in terms of the parameters of statistical theory so as to obtain the best fit to the data. Since considerable confusion on nomenclature exists in the literature, we consider it advisable to define the notation which we intend to use in this dissertation.

1. $\sigma_{n\gamma}$ = neutron capture cross section.
2. E = Energy of the incident neutron.
3. E_o = Energy at a resonance.
4. $\lambda\!\!\!^{-} = \lambda/2\pi = 1/k$ = Dirac wave length.
5. R = Radius of the target nucleus.
6. I = spin of the target nucleus.
7. ℓ = angular mom. of incident neutron.
8. $\underset{\sim}{J} = \underset{\sim}{I} + \underset{\sim}{\ell} + \underset{\sim}{1/2}$ = Spin of the compound nucleus.
9. $g_J = (2J+1)/2(2I+1)$ = statistical weight factor.

10. v_ℓ = penetration factor for neutrons of angular momentum ℓ. $v_0 = 1$, $v_1 = k^2R^2/(1+k^2R^2)$, $v_2 = k^4R^4/[9+3(kR)^2+(kR)^4]$

11. $\Gamma_n^{(\ell)}$ = Reduced neutron width at 1 ev of a resonance with angular momentum ℓ.

12. $\Gamma_n = \Gamma_n^{(\ell)}(\sqrt{E_o}v_\ell)$ = Neutron width of resonance at energy E_o with angular momentum ℓ.

13. Γ_γ = Gamma width of the resonance.

14. Γ = Total width of the resonance at energy E_o.

15. s = local level spacing in the neighborhood of a given resonance.

16. D_{obs} = (neutron energy interval)/(number of resonances of a given angular momentum ℓ in that interval).

17. $D_o = D_{obs} \times 2(2I+1)(2\ell+1)$.

18. $D_J = D_o/(2J+1)$

($D_J = D_o/2 = D_{obs}$ for $\ell = 0$, $I = 0$, and $J = 1/2$).

19. $\langle \Gamma_{nJ}^{(\ell)}/D_J \rangle = \langle \Gamma_n^{(\ell)}/D \rangle_J$ = neutron strength function for orbital angular momentum ℓ and spin J. In principle this quantity may be a function of J. However, in general, experimental numbers refer to the average over all J for a given ℓ (see 21 and 22). The parentheses ( ) are used when necessary to distinguish the index (ℓ) from an exponent.

20. $\langle \Gamma_\gamma/D_o \rangle_J \equiv (\bar{\Gamma}_\gamma/D_o)_J \equiv$ γ-ray strength function for spin J.

21. $\langle\langle \Gamma_{nJ}^{(\ell)}/D_J \rangle\rangle \equiv (2\ell+1)^{-1} \sum_J g_J \langle \Gamma_n^{(\ell)}/D \rangle_J \equiv \bar{\Gamma}_n^{(\ell)}/D$

22. $\langle\langle \Gamma_{\gamma J}/D_J \rangle\rangle \equiv \left[\sum_J g_J(2J+1)\right]^{-1} \sum_J g_J \langle \Gamma_\gamma/D \rangle_J \equiv \bar{\Gamma}_\gamma/D$

The average of a quantity is usually denoted by putting a bar at the top of it or <u>equivalently</u> by enclosing it in braces $\langle\ \rangle$. The two notations are used interchangeably, according to conven-

ience. Note that the symbol D always implies an average spacing.

Subscripts J and ℓ indicate that the given quantity refers to neutrons of a particular ℓ and resonances of a particular J which can be formed with those neutrons. Thus

$$\left[g_{J\ell}\left\langle\Gamma_\gamma/D_o\right\rangle_{J\ell}\right] = \left[g_J\left\langle\Gamma_\gamma/D_o\right\rangle_J\right]_\ell = \left[g\left\langle\Gamma_\gamma/D_o\right\rangle\right]_{J\ell} .$$

Subscripts are omitted whenever such omission does not lead to confusion.

If we neglect any multi-level effects and consider only the Breit-Wigner single level expression for capture then in the neighborhood of a resonance we may write

$$\sigma_{n\gamma} = g_J \pi \lambda\!\!\!^{-2} \Gamma_n \Gamma_\gamma / \left[(E_n - E_o)^2 + (\Gamma^2/4)\right] \qquad (1)$$

We can calculate the resonance integral by integrating $\sigma_{n\gamma}$ between the limits $E_o - s_J/2$ and $E_o + s_J/2$. Over this interval, which contains a single resonance, Γ_γ is constant and Γ_n is a slowly varying function of energy and can also be considered constant. Performing the integration and evaluating the constants, we obtain the average capture cross section of a single resonance over the interval s. This expression is:

$$\left\langle\sigma_{n\gamma}\right\rangle_{\ell J,\ \text{single reson.}} = 2\pi^2 \lambda\!\!\!^{-2} g_J \left(\Gamma_\gamma/s_J\right)\Gamma_n/(\Gamma_n + \Gamma_\gamma) \qquad (2)$$

The parameters Γ_γ, s, and Γ_n differ from level to level. If $\sigma_{n\gamma}$ is measured with a neutron spread $2\Delta E < D_{obs}$, resonance effects will be observed. However, we are now interested only in cases where $2\Delta E_n \approx 2$ kev $\gg D_{obs}$. and a smooth average capture cross section (as a function of energy) is observed which depends on the values of these parameters averaged over many levels.

Γ_γ is expected to vary little from level to level[24] but we obtain different expressions for $\bar{\sigma}_{n\gamma}$; depending on which one of the various suggested distributions for reduced neutron widths $\Gamma_n^{(\ell)}$ is chosen. The simplest assumption namely: $\Gamma_n^{(\ell)} = \bar{\Gamma}_n^{(\ell)}$ for all resonances yields:

$$\langle \sigma_{n\gamma} \rangle_{\ell J} = 2\pi^2 \lambda^2 g_J (\bar{\Gamma}_\gamma / D_J) \left[\bar{\Gamma}_n / (\bar{\Gamma}_n + \bar{\Gamma}_\gamma) \right]_J \qquad (3)$$

In general one gets

$$\langle \sigma_{n\gamma} \rangle_{\ell J} = 2\pi^2 \lambda^2 g_J (\bar{\Gamma}_\gamma / D_J) \left[\bar{\Gamma}_n / (\bar{\Gamma}_n + \bar{\Gamma}_\gamma) \right]_J F(\bar{\Gamma}_\gamma / \bar{\Gamma}_n)_J \qquad (4)$$

where $F(\bar{\Gamma}_\gamma / \bar{\Gamma}_n)$ is a correction factor determined by the choice of the probability distribution function for $(\Gamma_n^{(\ell)} / \bar{\Gamma}_n^{(\ell)})$ and is quite close to unity. The effect is illustrated for s-waves in Figure 3 and more generally in Figure 4 for exponential, i.e., $\exp(-\Gamma_n^{(\ell)} / \bar{\Gamma}_n^{(\ell)})$. distribution[25, 26] and the Porter-Thomas, i.e., $(\Gamma_n^{(\ell)} / \bar{\Gamma}_n^{(\ell)})^{-1/2} \exp(-\Gamma_n^{(\ell)} / 2\bar{\Gamma}_n^{(\ell)})$ distribution.[27]

At the present time the Porter-Thomas distribution of neutron widths is widely accepted since it has theoretical as well as partial experimental justification. The evaluation of $F(\bar{\Gamma}_\gamma / \bar{\Gamma}_n)_J$ using this distribution was done by E. G. Bilpuch[13] with the result:

$$F(\bar{\Gamma}_\gamma / \bar{\Gamma}_n) = (1+2b)^{-1} \left\{ 1 - 2\sqrt{b} \left[1 - H(\sqrt{b}) \right] / H'(\sqrt{b}) \right\}_J \qquad (5)$$

where $b = \bar{\Gamma}_\gamma / 2\bar{\Gamma}_n$ and $H(\sqrt{b}) = (2/\sqrt{\pi}) \int_0^{\sqrt{b}} e^{-t^2} dt$ and $H' = (2/\sqrt{\pi}) e^{-b}$ are the tabulated error function and its derivative.[28]

It may be noted that equation 4 is equivalent to the expressions obtained by Lane and Lynn[29] and Dresner[30] in a much more complicated manner.

The averaged capture cross section was calculated by summing the contributions of different spins, J, for each given ang-

ular momentum:

$$\langle \sigma_{n\gamma} \rangle = \sum_{\ell} \sum_{J} \langle \sigma_{n\gamma} \rangle_{\ell J} \qquad (6)$$

The simplest assumption for interpretation of capture cross sections ignores all but the s-wave contributions. This interpretation has been attempted even at energies as high as one Mev.[31] For many of the measured capture cross sections, the average s-wave parameters are known from fast chopper and other time-of-flight experiments in the ev region. The shape of the relative capture cross section curves can never be predicted with the assumption that only s-wave neutron capture is important, but for some nucleons the s-wave contribution predominates below about ten kev as may be seen from the results of detailed analysis to be discussed later. The next simplest assumption has been used with some success by Lane and Lynn.[29] They assumed that both the neutron and gamma strength functions are independent of neutron angular momentum and that the former has a value of about 10^{-4}. This assumption fits the observed capture cross sections of U^{238} quite satisfactorily above one hundred kev where three or more neutron orbital angular momenta ordinarily contribute appreciably to the capture cross section. However the dashed curve in Figure 3 (experimental data by E. G. Bilpuch[13]) shows that this simplifying assumption is unable to fit the trend of the experimental points in the neighborhood of twenty kev. The upper solid curve which fits the experimental points satisfactorily is a four parameter fit which ignores the contribution of d-waves. The lower solid curves show the separate s- and p-wave contributions. Estimates of the d-wave contribution indicate

that it is negligible in our energy region in most cases. This low value of the d-wave contribution U^{238} above forty five kev is due in part to competition between d-wave inelastic scattering and capture which is very unfavorable for the latter. At lower energies than are shown in Figure 3, the s-wave contribution decreases as $E^{-1/2}$, but at higher energies it is approaching an E^{-1} dependence asymptotically. The asymptotes of the p-wave contribution are also indicated in the figure. The dotted line in Figure 3 shows that it makes little difference whether a Porter-Thomas or an exponential distribution is chosen for the s-wave component; similar calculations show that the same is true for the p-wave component. From Figure 4, page 30, it can be seen that the curve fitting would not even be affected greatly if the distribution of neutron widths were ignored completely. In all our discussion, we actually assume the Porter-Thomas distribution.

There are two p-wave and one s-wave channels for an even-even target nucleus and twice as many when the spin of the target is one or more. Hence, there are six to twelve possible free parameters in equation 6. It is impossible to obtain so many parameters from the average capture cross section data without simplifying assumptions. If it is assumed that the strength function is the same for all J values of a particular neutron angular momentum, the strength function becomes $\bar{\Gamma}_{nJ}^{(\ell)}/D_J = \bar{\Gamma}_n^{(\ell)}/D$. The assumption is probably correct for many cases (including s-waves) but it should not be valid if there is an appreciable spin-orbit coupling effect[32, 33] for p-wave neutrons.

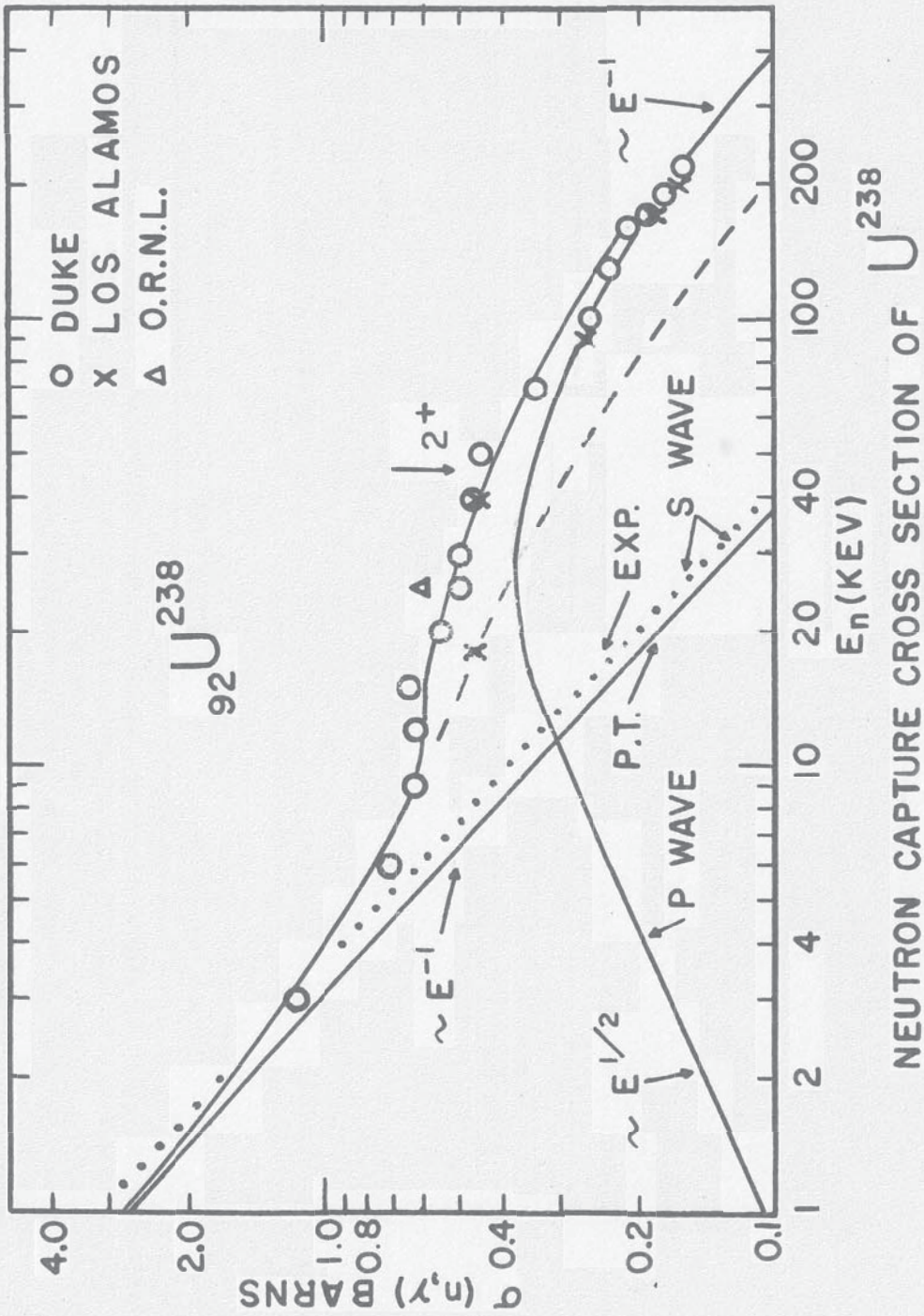
O DUKE
X LOS ALAMOS
Δ O.R.N.L.
92U238
2+
~E-1
EXP.
P.T.
S WAVE
P WAVE
~E1/2
~E-1
σ (n,γ) BARNS
4.0
2.0
1.0
0.8
0.4
0.2
0.1
1
2
4
10
20
40
100
200
En(KEV)
NEUTRON CAPTURE CROSS SECTION OF U238

Figure 3

In that case a weighted average: $\bar{\Gamma}_n^{(\ell)}/D=(2\ell+1)^{-1}\ \Sigma_J(g\bar{\Gamma}_n^{(\ell)}/D)_J$ is called the p-wave strength function. It is also of interest to inquire into the J dependence of the parameters $\bar{\Gamma}_\gamma/D_J$ and $\bar{\Gamma}_\gamma/D_o$. Stolovy and Harvey[34] find empirically that $\bar{\Gamma}_\gamma/D_J$ is proportional to $(2J+1)^{-5/4}$ in accordance with a suggestion of Lang and LeCouteur.[35] Assuming a 2J+1 dependence for D_J, Γ_γ/D_o is at most proportional to $(2J+1)^{-1/4}$. Because of this weaker J dependence, we have chosen to call $(\bar{\Gamma}_\gamma/D_o)$ the γ-strength function and for the purpose of our analysis considered it independent of J and E_n for a given neutron angular momentum. Since it is generally considered that $\bar{\Gamma}_{nJ}^{(\ell)}/D_J$ is independent of J, if we assume a 2J+1 dependence on D_J a similar J dependence must be assumed for $\bar{\Gamma}_{nJ}^{(\ell)}$.

The above assumptions reduce the free parameters in equation 6 to four: $\bar{\Gamma}_n^{o}/D$, $\bar{\Gamma}_n^{(1)}/D$, $(\bar{\Gamma}_\gamma/D_o)_s$, and $(\bar{\Gamma}_\gamma/D_o)_p$. Clearly the relative cross section curves (which are actually measured) may be described by only three. The values of the parameters $(\bar{\Gamma}_\gamma/D_o)_s$ and $\bar{\Gamma}_n^{o}/D$ are obtained from total cross section measurements whenever they are available; the object of the analysis is to determine the p-wave parameters as well as possible.

It is generally found possible to fit a capture cross section curve under the assumption that the gamma ray strength functions are the same for s- and p-wave neutrons when the mass number of the target nucleus is odd. On the other hand, when the target is even-even as in U^{238} and Pd^{108} one must assume that the p-wave gamma ray strength function differs from that of the

s-wave by a large margin. For instance, the poor fit (Figure 3, page 25) to the U^{238} cross section under the assumption that the two δ-strength functions are equal cannot be improved by any reasonable changes in the other parameters. It has been customary in the past to assume that the s- and p-wave gamma ray strength functions are equal, and it does seem reasonable that the radiation width (which is a statistical average over a large number of gamma ray transitions) should not differ between s- and p-wave neutrons. However, it is quite reasonable that the level densities, D_o^{-1}, should depend on the parity of the entering neutron.

Consider, for instance, a model similar to that studied by Newson and Duncan. If the paring energy in the compound nucleus is very high, an s-wave neutron entering the U^{238} nucleus can only fall into the $4s^{1/2}$ level (which is the top subshell of the major shell between 126 and 184 neutrons) whereas a p-wave neutron must fall into the $4p^{1/2}$ or $4p^{3/2}$ subshells which are in the 82-126 shell. If the effective paring energy is sufficiently high (which appears to be the case[36]) the predominant mode of excitation of the compound nuclei will be an excitation of indistinguishable pairs of protons and neutrons. For the captured neutron to go into one of the negative parity states of the compound nucleus, a neutron pair must be excited into the next higher major shell to make room for the negative parity unpaired neutron. While this process requires a good deal of energy, the s-wave neutron in the $1/2^+$ state is also far above the lowest energy subshell which it might occupy if there were no selection

rules, thus capture into any of the three possible levels is about equally unfavorable energetically. Under these circumstances the ratio of level densities for the s- and p-wave cases is simply the ratio of the number of configurations into which indistinguishable pairs may be partitioned without exciting any pair from one major shell to another. This calculation indicates that the level density (D_o^{-1}) for either the $1/2^-$ or $3/2^-$ p-wave compound nucleus, U^{239}, should be about three times that of the s-wave ($1/2^+$), in good agreement with the measured ratio. While we have taken a much simplified model for our example, it is sufficient to indicate the possibilities of difference in level densities depending on the parity of the bombarding neutron.

If an odd proton or neutron had been present in the target nucleus it could change its parity without the expenditure of a great deal of energy, so that the parity effect should be much less important in the case of an odd A target. Thus we can understand on the basis of the shell model that the gamma ray strength functions appear to be the same for s- and p-wave neutrons when the target is odd and are often quite different when the target is even-even. In fitting the relative capture cross section curve for a nucleus of odd mass number, there are then only two effective parameters: the s-wave strength function (usually known from total cross sections) and the p-wave strength function which is then easily determinable in favorable cases.

For analysis of the experimental data, it was found easier to work with equation 6 divided by $2\pi^2\lambda^2$. In this form each channel of the s-wave contribution is approximately equal to

$g_J(\bar{\Gamma}_n^{\circ}/D_J)E^{1/2}$ at low energy, and at higher energies reaches the asymptote, $g_J(2J+1)(\bar{\Gamma}_\gamma/D_o)$. A general curve may be drawn on log-log paper by plotting $\sigma(n,\gamma)_{J,s}$ divided by $2\pi^2\lambda\!\!\!^{-2}g_J(\bar{\Gamma}_\gamma/D_J)$ versus the parameter, $(\bar{\Gamma}_n^{\circ}/\bar{\Gamma}_\gamma)^2E$. This curve is valid for any s-wave channel.

If $I \neq 0$, there are two s-wave channels. With the assumptions given on the previous page, "general curves" for both channels can be added so that a curve of $(2\pi^2\lambda\!\!\!^{-2}\,\bar{\Gamma}_\gamma/D_o)^{-1}\langle\sigma_{n\gamma}\rangle_s$ versus $[(2J+1)\,\bar{\Gamma}_n/\bar{\Gamma}_\gamma]^2$ can be plotted for a given target spin, and this plot used to generate $(2\pi^2\lambda\!\!\!^{-2})^{-1}\langle\sigma_{n\gamma}\rangle_s$ versus E_n for any set of s-wave parameters. Such a plot is illustrated in Figure 4 for the case $I = 1/2$.

The general p-wave contribution to $(2\pi^2\lambda\!\!\!^{-2}\,\bar{\Gamma}_\gamma/D_o)^{-1}\langle\sigma_{n\gamma}\rangle$ for a particular target spin was plotted versus $[(2J+1)\bar{\Gamma}_n/\bar{\Gamma}_\gamma]^{2/3}$. In this case the latter parameter is proportional to $E_n[1+(kR)^2]^{-2/3}$, where $k = 1/\lambda\!\!\!^{-}$ and $R = 1.35A^{1/3}$ fermis. This distortion of the energy scale which is negligible below fifteen kev does not lead to any difficulty.

Using the above "general curves" for s- and p-wave neutrons for a particular target spin, it is easily seen that to a good approximation (within a few per cent), the J dependence of D_J is important only so far as the absolute value of $(\bar{\Gamma}_\gamma/D_o)$ is concerned. The change in shape of $\langle\sigma_{n\gamma}\rangle_\ell$, due to this assumption is negligible. This fact is illustrated in the upper curve of Figure 4, where the open circles are the calculated total s-wave contributions for the case $I = 1/2$ with the assumption that both $\bar{\Gamma}_\gamma/D_o$ and $\bar{\Gamma}_n^{\circ}/D$ are the same for both $J = 0$ and 1.

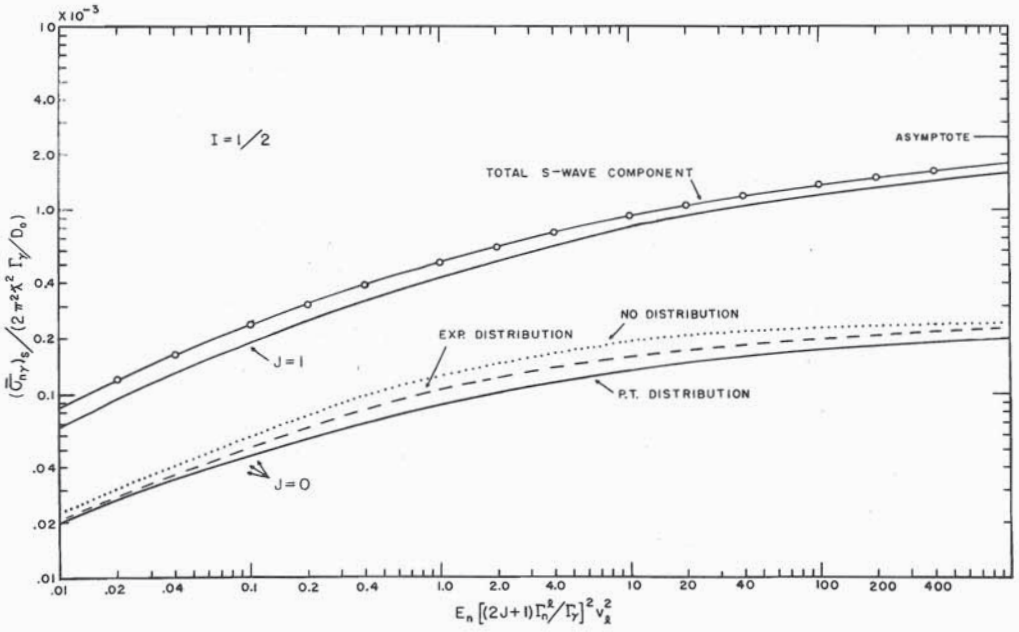

GENERAL S-WAVE CONTRIBUTION FOR I=1/2 TARGET NUCLEUS

FIGURE 4

The upper solid line has the shape, but not the absolute value (different average parameters) of a single s-wave J contribution. Similar considerations for p-wave neutrons lead to the same conclusions. For $I > 3/2$, even the J dependence of D_J becomes unimportant compared to other uncertainties.

With the above "general curves" for a particular target spin, the analysis of the average capture cross sections proceeded as follows:
(a.) A plot of the experimental $(2\pi^2\lambda^2)^{-1}\langle\sigma_{n\gamma}\rangle$ versus E_n was made on log-log tracing paper. (b.) The best known s-wave parameters from other experiments were used to match the scales of the "general s-wave curve for the particular target spin "with those of $(2\pi^2\lambda^2)^{-1}\langle\sigma_{n\gamma}\rangle$ versus E_n, and the s-wave contribution was traced on the experimental curve. (c.) The above two curves were subtracted to yield $(2\pi^2\lambda^2)^{-1}\langle\sigma_{n\gamma}\rangle_p$ versus E_n, and the difference was plotted versus the slightly distorted energy scale, $E_n[1+(kR)^2]^{-2/3}$. (d.) The p-wave parameters were determined by sliding the p-wave general curve until a good fit is obtained.

If after the s-wave contribution was subtracted, the curve did not have the characteristic p-wave shape over the proper energy range, the s-wave parameters were adjusted. This is a necessary procedure to fit the capture cross sections since there are always appreciable uncertainties in both the s-wave parameters and the absolute cross section.

Other workers[37, 38, 39] have programed equation 6 for various computers so that the experimental capture cross sections

could be fitted by adjusting parameters. The comparatively simple and flexible manual analysis described above was developed in order to obtain a better physical insight into the curve fitting process.

While it is convenient to normalize our relative cross sections to the most reasonable measurement of absolute cross section available and then to use s-wave parameters to subtract off the s-wave contribution to the capture cross section, it is obvious from examination of equation 6 that certain ratios of parameters may be determined purely from the shape of the relative cross section curve and independent of both the absolute capture cross section and the s-wave γ-strength function. The following ratios of parameters may always be determined independently of the absolute cross sections or the s-wave parameters: $(\bar{\Gamma}_\gamma/D_o)_p/(\bar{\Gamma}_\gamma/D_o)_s$ and $\langle \Gamma_n^{(1)}/D \rangle_p / \langle \Gamma_\gamma/D_o \rangle_s$. The first ratio is interesting in itself in that it appears to throw some light on the effect of neutron parity on resonance spacing as was discussed earlier. From the second ratio we can determine the p-wave strength function if the s-wave γ-strength function is known. Even when neither the absolute cross section nor the s-wave γ-strength function is known, one can sometimes determine the ratios: $\langle \Gamma_n^{(1)}/D \rangle_p / \langle \Gamma_n^{(o)}/D \rangle_s$ and $\langle \Gamma_n^{(o)}/D \rangle_s / \langle \Gamma_\gamma/D_o \rangle_p$, from which a value of the p-wave neutron strength function may be obtained even though the absolute value of the cross section is not known. This seems to be the case for the cross section of Au^{197} which will be discussed later. The second two ratios are not always determinable, i.e., it sometimes happens that,

even at the low energy end of the cross section curve, $\overline{\Gamma}_n$ for s-waves is so much larger than $\overline{\Gamma}_\gamma$ that the former nearly cancels out and the capture cross section becomes almost independent of the s-wave neutron strength function. Also it sometimes happens that the shape of the relative curve is too simple (as will be discussed later) to determine so many parameters. Hence the uncertainty of the p-wave strength function determined by our analysis is rather large if only the s-wave strength function is available for normalization, but since the s-wave neutron strength function is practically always known either from direct measurement or interpolation, a useful estimate of $\overline{\Gamma}_n^{(1)}/D$ is usually possible. The estimate is much more reliable if $(\overline{\Gamma}_\gamma/D_o)_s$ is known, but when absolute cross section information is also available inconsistencies frequently appear; it is usually possible to eliminate them by adjusting the given parameters within their experimental errors, but in a few cases no value of the p-wave strength function can be found which is reasonably consistent with all the available data. It is clear that the accuracy of the p-wave strength functions will improve as the quality and quantity of the supplementary data increases.

The uniqueness of the results of analysis will now be discussed. If the slope of the $\overline{\sigma}_{n\gamma}$ versus E plot changes abruptly, and the change can be ascribed to the participation of p-wave neutrons (d-wave neutrons do not usually contribute appreciably below a hundred kev) then the p-wave parameters can be determined to within $\pm$ 50 percent from the shape and absolute cross section alone, without prior accurate knowledge of s-wave parameters

(see Figure 6, page 38). However, in certain cases (see Figure 10, page 40) the cross section is very nearly smooth and monotonically decreasing. In such cases s- and p-wave decomposition is not easy and its uniqueness is determined by the accuracy of the known s-wave parameters. In all cases the large quoted errors are indicative of this uncertainty, and the uncertainty in absolute normalization.

In order to compare the p-wave strength function results with optical model theory, the results from total cross section measurements have also been considered. Newson et al[11] have estimated $\bar{\Gamma}_n^{(1)}/D$ from the total cross section measurements on rather thin samples. In order to simplify analysis they assumed that s-wave resonance contributions were negligibly small and that $\bar{\Gamma}_n \gg \bar{\Gamma}_\gamma$. Neither of these assumptions is very accurate at lower energies. Recently, however, we have developed more general methods of analysis which do not use any of the above simplifications. Experimental values of s-wave strength functions are used, a more accurate expression for potential scattering cross section employed,[40] and area analysis curves with appropriate correction[41] are used in such a manner that no assumption about relative magnitudes on $\bar{\Gamma}_n$ and $\bar{\Gamma}_\gamma$ is required. This method, which will be described in detail elsewhere,[42] is being tried on a number of nuclei under various experimental conditions and here we present only preliminary results obtained for the nuclei in our region of interest.

Chapter III

INTERPRETATION OF EXPERIMENTAL RESULTS

The experimental results for capture cross sections are illustrated in Figures 3 and 5 through 14. The theoretical curves shown in these figures were calculated according to equation 6 using the parameters listed in Table II, page 58. The values of the s-wave parameters used in the analysis as well as the measured values are listed with reference. These data agree within quoted errors but are not exactly the same.

For a brief discussion of individual nuclei, we divide the capture cross section measurements into two groups. The first group includes those nuclei for which unique results could be obtained by analysis of the capture cross section. The second group may be called the "problem group."

GROUP I

Molybdenum^{100}: The s-wave parameters for Mo^{100} isotope are

not known. Only those of the aggregate of even-even Mo isotopes[10] are known with large uncertainty. As will be seen later, at least the knowledge of the upper limit of the p-wave strength function for Mo^{100} is very important in the theoretical considerations to be discussed. Using the lowest possible value of $(\bar{\Gamma}_\gamma/D_o)_s = 1.0 \times 10^{-4}$ and assuming $(\bar{\Gamma}_\gamma/D_o)_s = (\bar{\Gamma}_\gamma/D_o)_p$ an upper limit of $\bar{\Gamma}_n^{(1)}/D = 2.0 \times 10^{-4}$ was obtained. Figure 5 illustrates the fit to the experimental data with the same assumptions concerning $(\bar{\Gamma}_\gamma/D_o)$ and the "best fit" value of the p-wave strength function which is $\bar{\Gamma}_n^{(1)}/D = 1.0 \times 10^{-4}$. Good fits with $\bar{\Gamma}_n^{(1)}/D < 1.0 \times 10^{-4}$ are obtained if higher values of $(\bar{\Gamma}_\gamma/D_o)_s$ are chosen. Such choice, however, necessarily requires $(\bar{\Gamma}_\gamma/D_o)_p < (\bar{\Gamma}_\gamma/D_o)_s$, a result which is not difficult to understand in terms of parity effects on s- and p-wave level spacings. As can be seen in Figure 5 the relative capture cross section data was normalized to the absolute measurements of Leipunsky et al.[43] and Johnsrud et al.[44] Absolute measurements by Macklin et al.[45] and Vervier[46] are shown for comparison.

Silver^{107}: The s-wave parameters of Ag^{107} have been measured by a number of groups[47, 48, 49] and are in agreement with those derived from natural silver[50]. From Figure 6 it is seen that an excellent fit is obtained using these parameters. The largest value of $(\bar{\Gamma}_\gamma/D_o)_s$, consistent with the uncertainties of the measurement was chosen to fit the data and $(\bar{\Gamma}_\gamma/D_o)_p \simeq (\bar{\Gamma}_\gamma/D_o)_p$ was assumed. The absolute $\bar{\sigma}_{n\gamma}$ measurements used for normalization are by Macklin et al.[45, 51] at

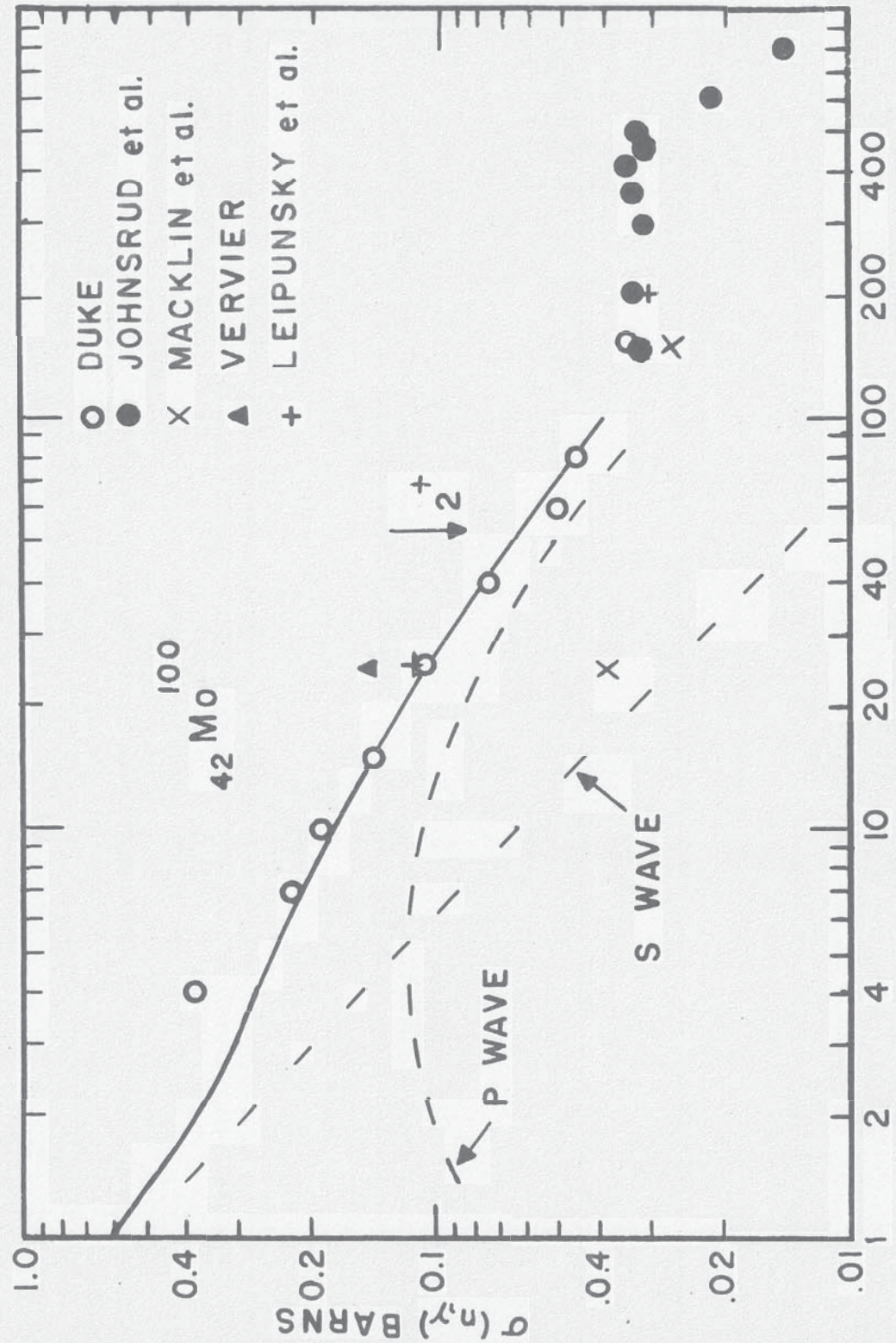
DUKE
JOHNSRUD et al.
MACKLIN et al.
VERVIER
LEIPUNSKY et al.
$^{100}_{42}Mo$
2^+
P WAVE
S WAVE
$\sigma(n,\gamma)$ BARNS
E_n(KEV)
NEUTRON CAPTURE CROSS SECTION OF Mo^{100}

Figure 5

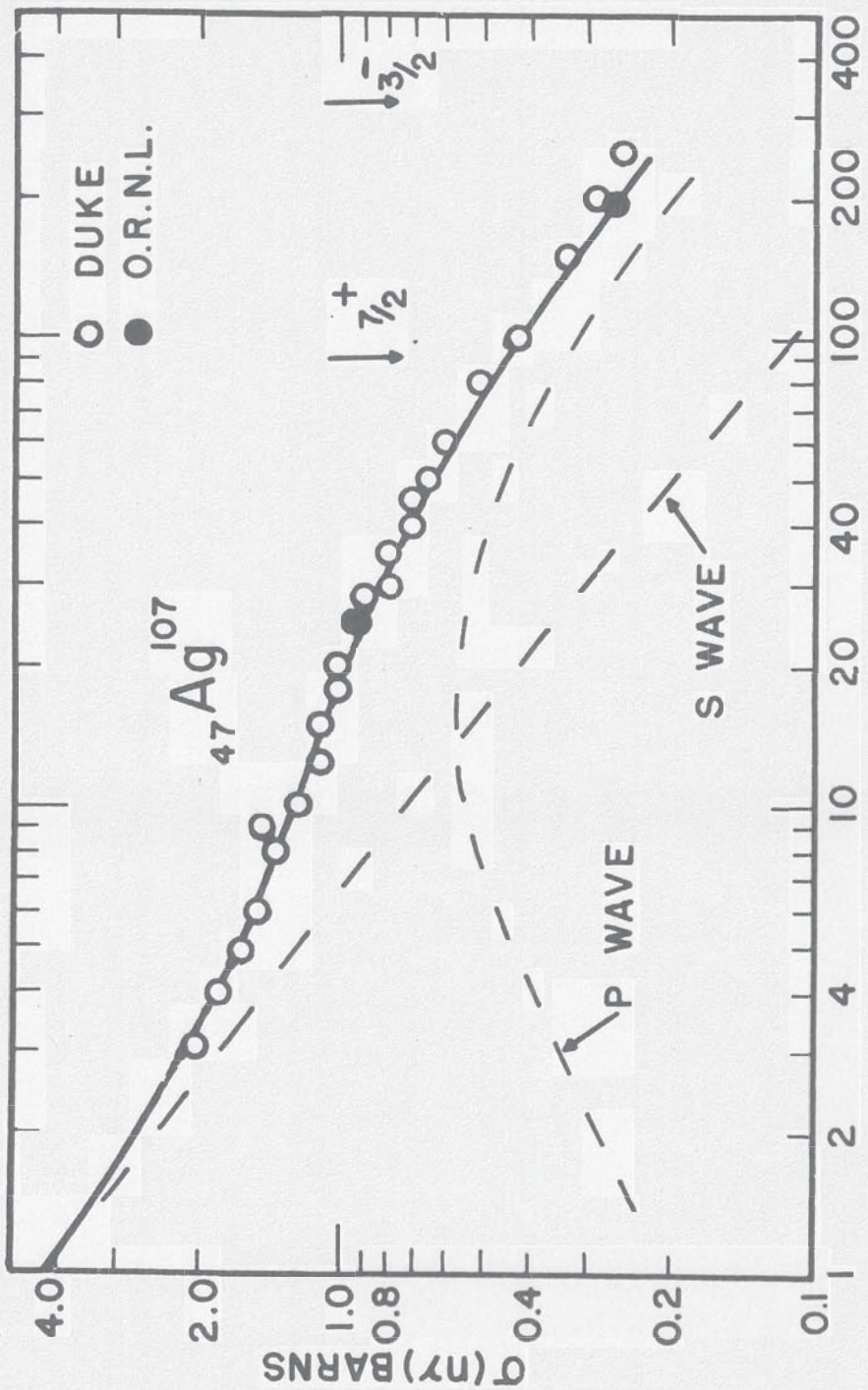

NEUTRON CAPTURE CROSS SECTION OF Ag^{107}

Figure 6

at Oak Ridge National Laboratory.

Silver^{109}: By fitting the shape of the relative capture cross section of Ag^{109} with well known s-wave parameters[47,48,49] and the assumption that $(\bar{\Gamma}_\gamma/D_o)_p = (\bar{\Gamma}_\gamma/D_o)_s$, absolute values of the cross section are obtained which are in good agreement with those obtained by subtracting the Ag^{107} cross sections[37, 45,44] from that of natural silver.[52] This fit is illustrated in Figure 7. It is inferred that for Ag all the absolute cross sections due to Linenberger et al.[2] are too high by an approximate factor of two. If we use their absolute values we are required to assume a $(\bar{\Gamma}_\gamma/D_o)_s$ at least about a factor of four larger than the measured value.

Indium^{115}: The relative capture cross section for the formation of the 54 min. isomeric state was measured and is shown in Figure 8. Absolute $\sigma_{n\gamma}$ measurements used for normalization are by Macklin, et al.[45] at Oak Ridge National Laboratory and by Johnsrud et al.[44] at the University of Wisconsin. This cross section was raised by 16 percent to account for the cross section of the 13 sec. half life ground state[1] (assumed to have same shape). The normalization for the total absorption cross section was thus used for analysis. Using known s-wave parameters, and $(\bar{\Gamma}_\gamma/D_o)_p = (\bar{\Gamma}_\gamma/D_o)_s$ the p-wave strength function is found to be in the range $(1.25\text{-}4.0) \times 10^{-4}$ with the most probable value of $\bar{\Gamma}_n^{(1)}/D = 2.0 \times 10^{-4}$.

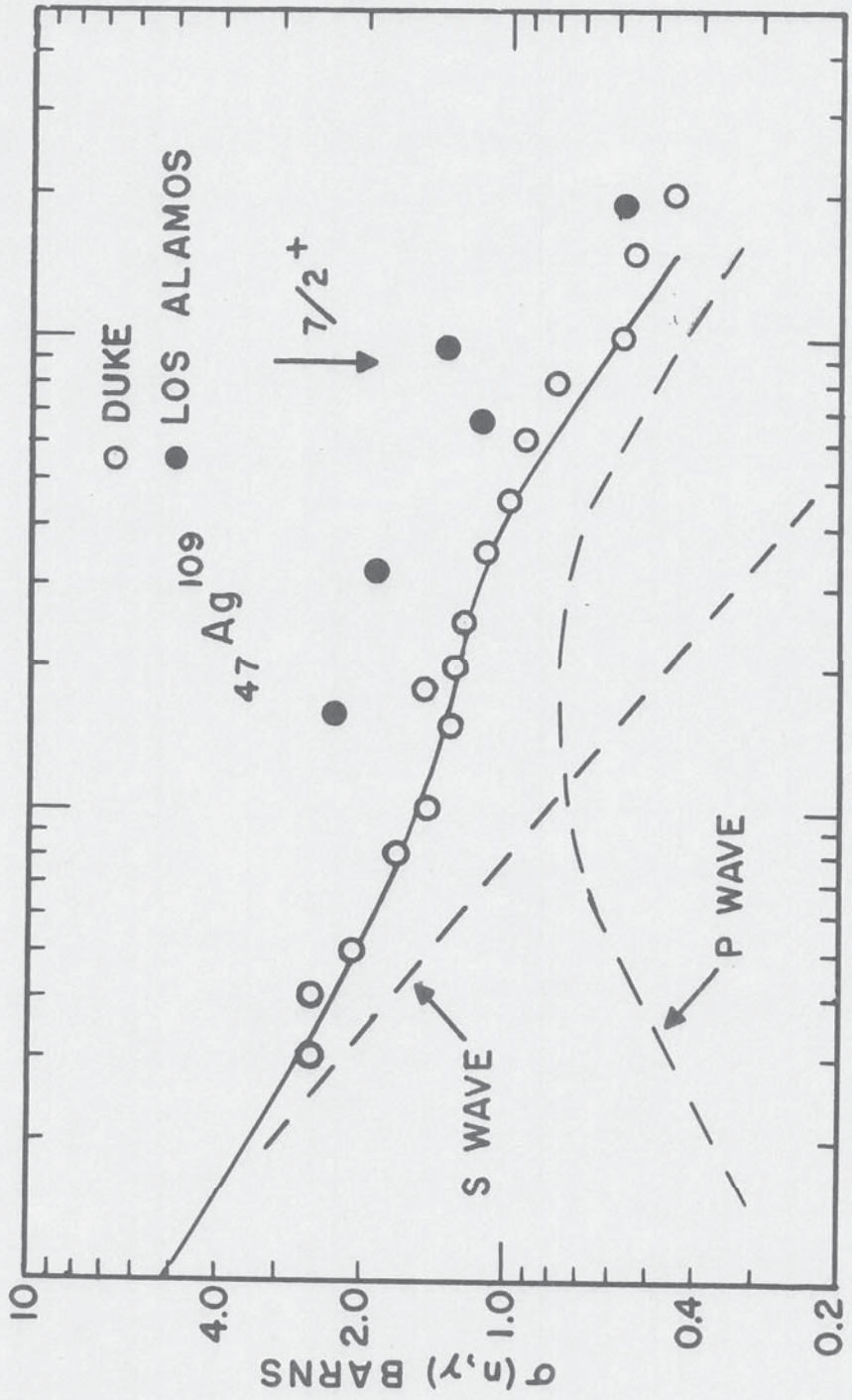
O DUKE
● LOS ALAMOS
$_{47}Ag^{109}$
7/2+
S WAVE
P WAVE
σ (n,γ) BARNS
10
4.0
2.0
1.0
0.4
0.2
1
2
4
10
20
40
100
200
E_n(KEV)
NEUTRON CAPTURE CROSS SECTION OF Ag^{109}

Figure 7

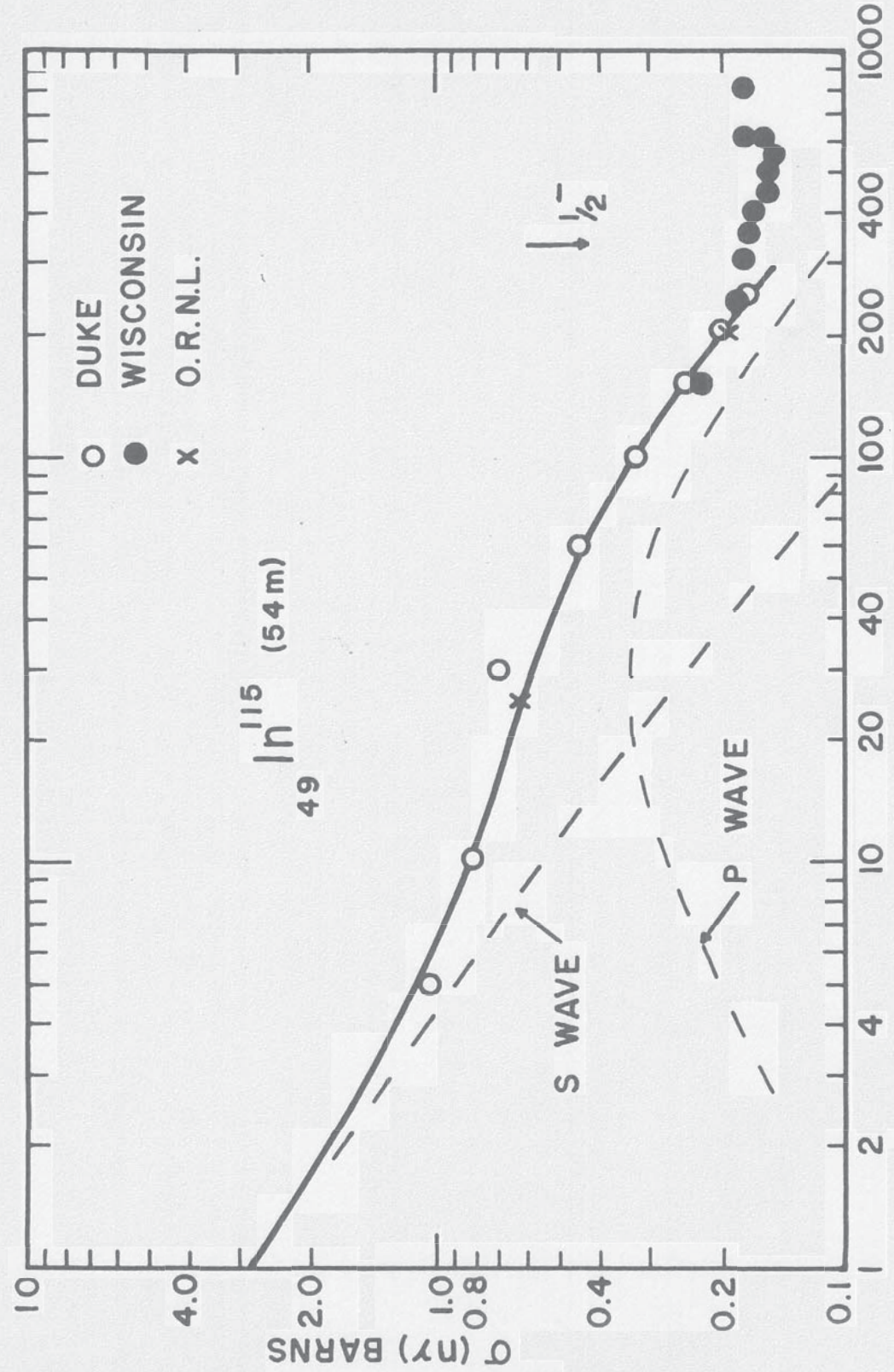
DUKE
WISCONSIN
O.R.N.L.
In^{115}_{49} (54m)
$I_{1/2}^-$
S WAVE
P WAVE
σ (nγ) BARNS
En(KEV)
NEUTRON CAPTURE CROSS SECTION OF In^{115}

Figure 8

Iodine^{127}: The capture cross section measurements on Iodine are shown in Figure 9. The relative measurements were normalized to the work of Booth et al.,[53] Macklin et al.,[45] and Johnsrud et al.[44] A good fit could be obtained with s-wave parameters consistent with experimentally determined values and the assumption that $(\bar{\Gamma}_\gamma/D_o)_p = (\bar{\Gamma}_\gamma/D_o)_s$.

Uranium^{238}: The experimental data on U^{238} was not done by the author but by Dr. E. G. Bilpuch.[13] This data has been included in this dissertation only for the purpose of the previous discussion. The fit to the U^{238} data shown in Figure 3, page 25, is insignificantly different from that shown in Bilpuch's thesis.

GROUP II

Arsenic^{75}: The absolute capture cross section of As^{75} has been measured by three different groups[45, 53, 44] and their results are in excellent agreement. The relative measurements normalized to these determinations are shown in Figure 10. Unless all these measurements are too high by an approximate factor of two, it is not possible to fit our data with the known parameters. Two different measurements[8, 9] of $\bar{\Gamma}_n^o/D$ are in good agreement, so that the discrepancy is attributed to the measured value of $(\bar{\Gamma}_\gamma/D_o)_s$. In the fit shown in Figure 10 this value was ignored and it was assumed that $\bar{\Gamma}_n^{(1)}/D = 10^{-4}$, the upper limit consistent with total cross section measurements. Under this assumption $(\bar{\Gamma}_\gamma/D_o)_s$ must be larger than the measured

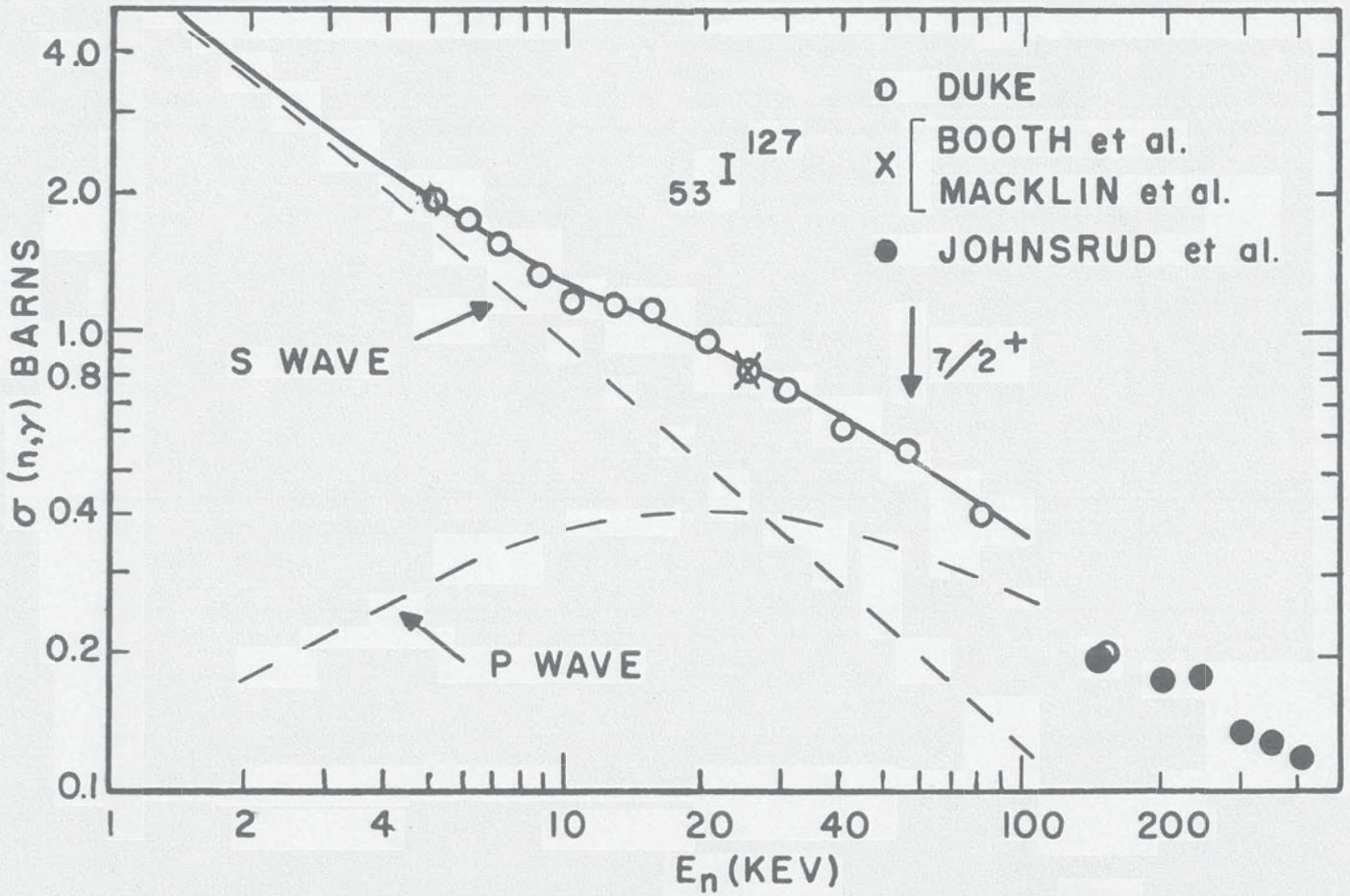

NEUTRON CAPTURE CROSS SECTION OF I^{127}

Figure 9

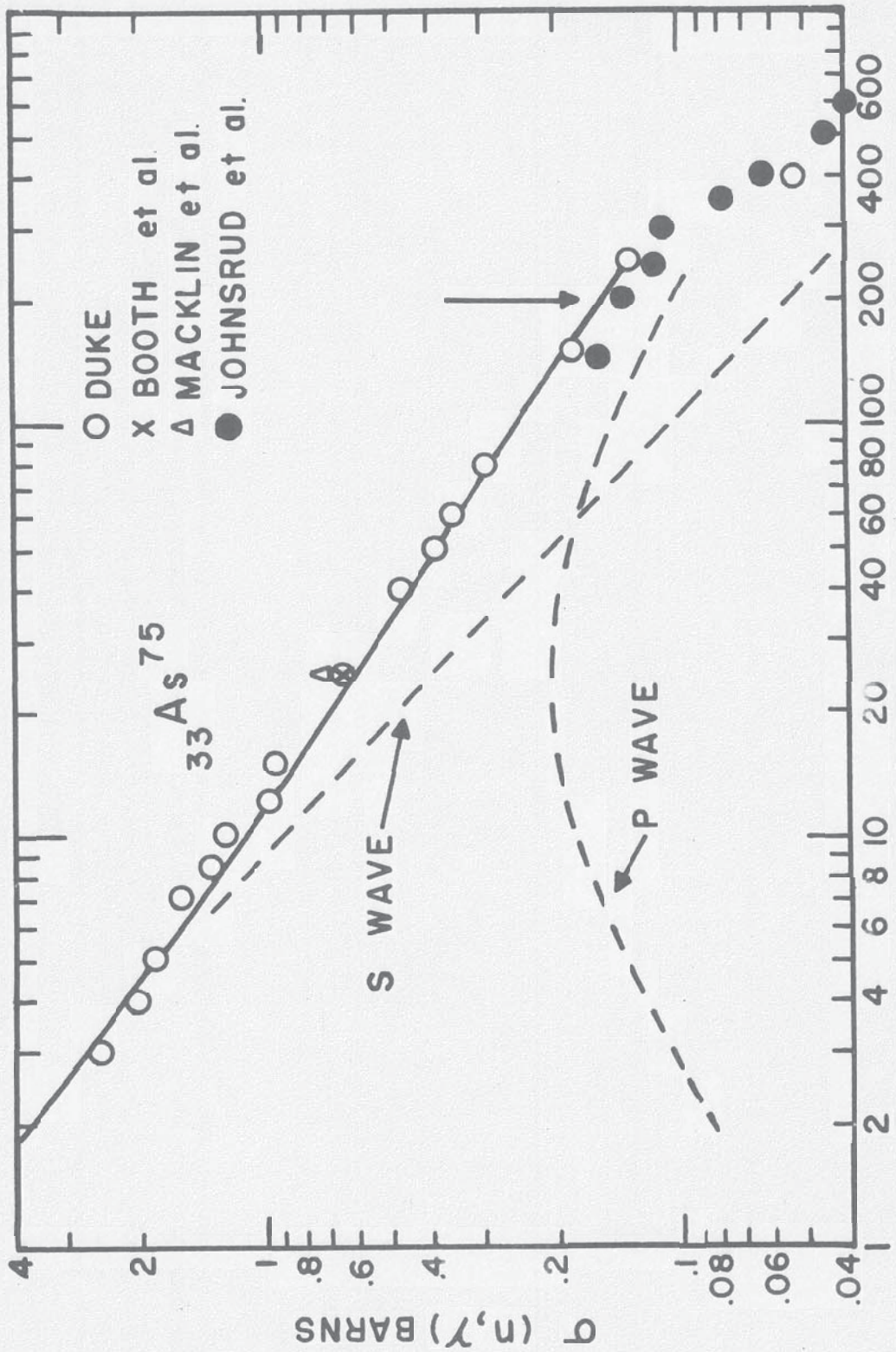
O DUKE
X BOOTH et al.
Δ MACKLIN et al.
● JOHNSRUD et al.
33 As 75
S WAVE
P WAVE
σ (n,γ) BARNS
E_n (KEV)
NEUTRON CAPTURE CROSS SECTION OF As 75

Figure 10

value by a factor of 2.3.

Rhodium^{103}: The relative capture cross sections for the 44 sec. ground state and the 4.4 min. isomeric state were measured and were found to have the same shape. No absolute capture cross section measurements for Rh^{103} are available at 25 kev, where they are particularly sensitive to p-wave effects. Diven and Terrell's[54] results at 180 kev are the basis of the scale in Figure 11. Further, s-wave parameters of Rh^{103} are very poorly known.[34] Hence it is possible to estimate $\bar{\Gamma}_n^{(1)}/D$ only roughly. We have not attempted to show the rather arbitrary fit in Figure 11. We can however estimate (see Figure 15) that $\bar{\Gamma}_n^{(1)}/D$ lies within the range (1.0 to 4.0) x 10^{-4}.

Palladium^{108}: S-wave parameters for the Pd^{108} isotope are not known. Only rough estimates of s-wave parameters can be made from total cross section data on the natural element[55] since Pd^{108} is a minor isotope.

A fit to the capture cross section of Pd^{108} which is consistent with the poorly known s-wave parameters is shown in Figure 12, where the relative data is normalized to the absolute measurements of Macklin et al.,[45] and Booth et al.[53] Due to the lack of accurate s-wave parameters and to the monotonically decreasing nature of the observed capture cross section, a unique fit was not possible. It was found that all reasonable fits required the condition $(\bar{\Gamma}_\gamma/D_o)_p < (\bar{\Gamma}_\gamma/D_o)_s$. The p-wave strength function could only be determined within a very large error which is shown in Figure 15, page 53.

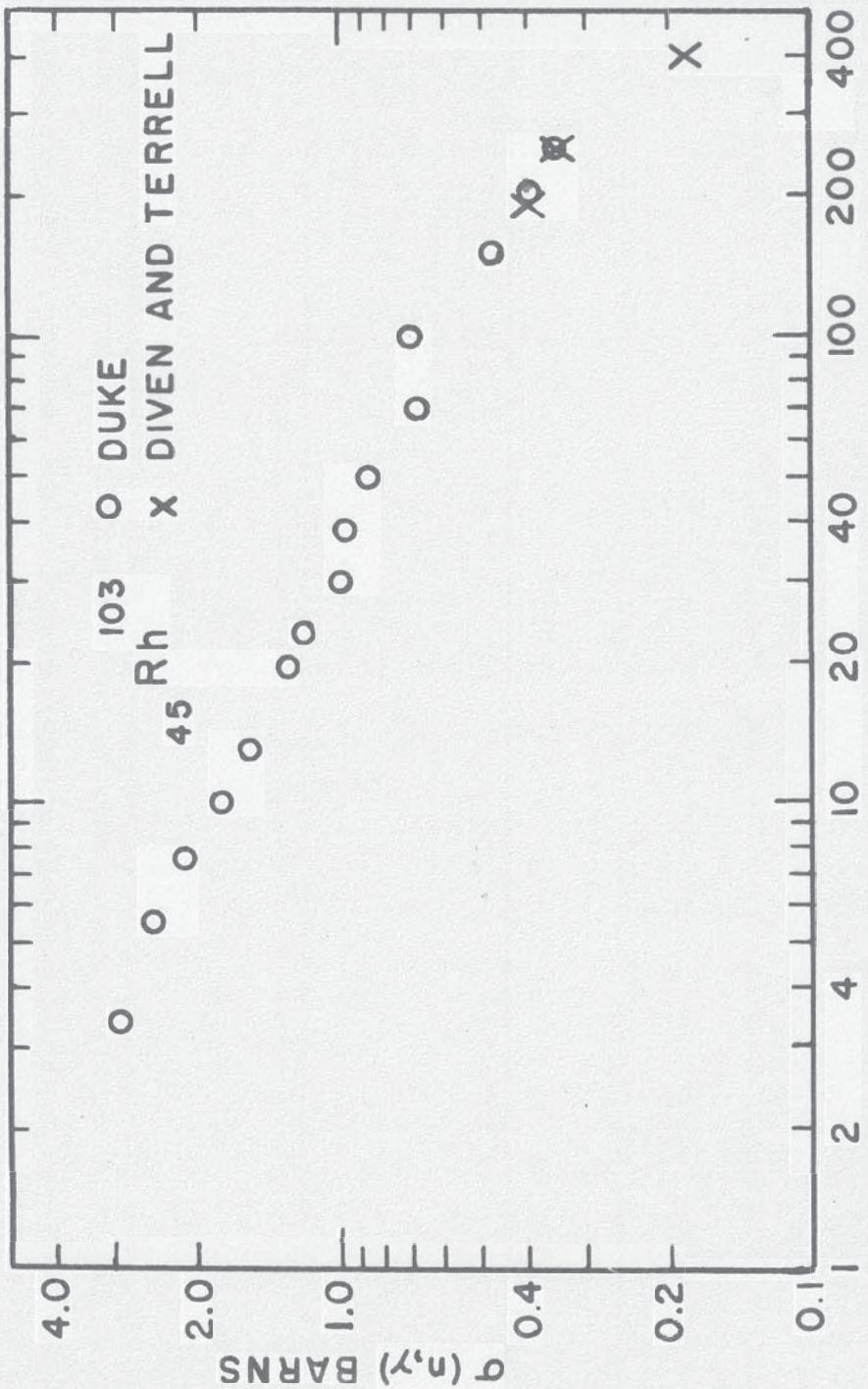
NEUTRON CAPTURE CROSS SECTION OF Rh 103
E_n(KEV)
σ (n,γ) BARNS
4.0
2.0
1.0
0.4
0.2
0.1
1
2
4
10
20
40
100
200
400
103 Rh 45
O DUKE
X DIVEN AND TERRELL

Figure 11

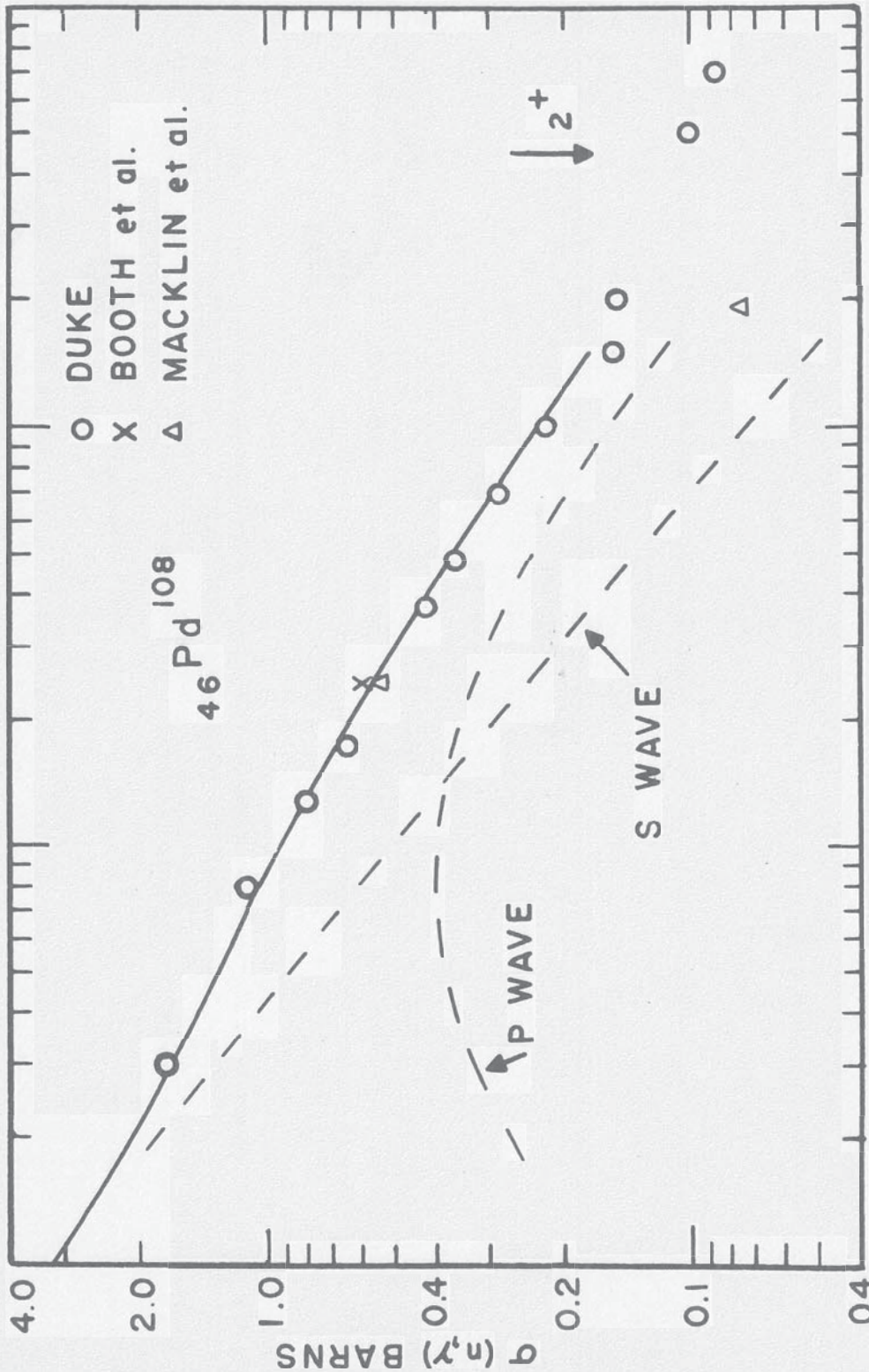
NEUTRON CAPTURE CROSS SECTION OF Pd108
46Pd108
O DUKE
X BOOTH et al.
Δ MACKLIN et al.
2+
P WAVE
S WAVE
σ (n,γ) BARNS
En(KEV)
4.0
2.0
1.0
0.4
0.2
0.1
.04
1
2
4
10
20
40
100
200
400

Figure 12

Gold^{197}: Gold belongs to the problem group because of inadequate knowledge of the absolute capture cross section. Since gold is monoisotopic with a convenient half life for β decay, many experimenters have attempted measurements of the absolute capture cross section but the agreement is very poor (see BNL-325.[15]

The data shown in Figure 13 is normalized to measurements by Booth et al. (U.C.R.L.)[53] and Johnsrud et al. (WISCONSIN).[44] With this normalization, the fit to the experimental data is in very poor agreement with the measured value of $(\bar{\Gamma}_\gamma/D_{obs.})_s$ (see Table II, page 58). Very recent measurements indicate that agreement is proceeding from both directions, i.e., very recent unpublished results of H. W. Schmitt and C. W. Cook of Oak Ridge National Laboratory using the shell transmission method indicate that the capture cross section at 25 kev is only 585 ± 60 mb and very recent estimates of $\bar{\Gamma}_\gamma$ for gold are higher than the previously accepted valve.[56] Both of the above values bring the measured s-wave parameters and the absolute capture cross section into better agreement.

As has already been discussed, the value of $\bar{\Gamma}_n^{(1)}/D$ determined and $(\bar{\Gamma}_\gamma/D_o)_p = (\bar{\Gamma}_\gamma/D_o)_s$ is relatively independent of the above discrepancies.

Platinum^{198}: The average capture cross section curve for Pt^{198} is shown in Figure 14. Our curve has been normalized to the average of two absolute measurements at 25 kev by Hummel and Hamermesh[57] and Booth et al.[53] The sharp break that occurs around forty kev appears to be a dramatic example of partial

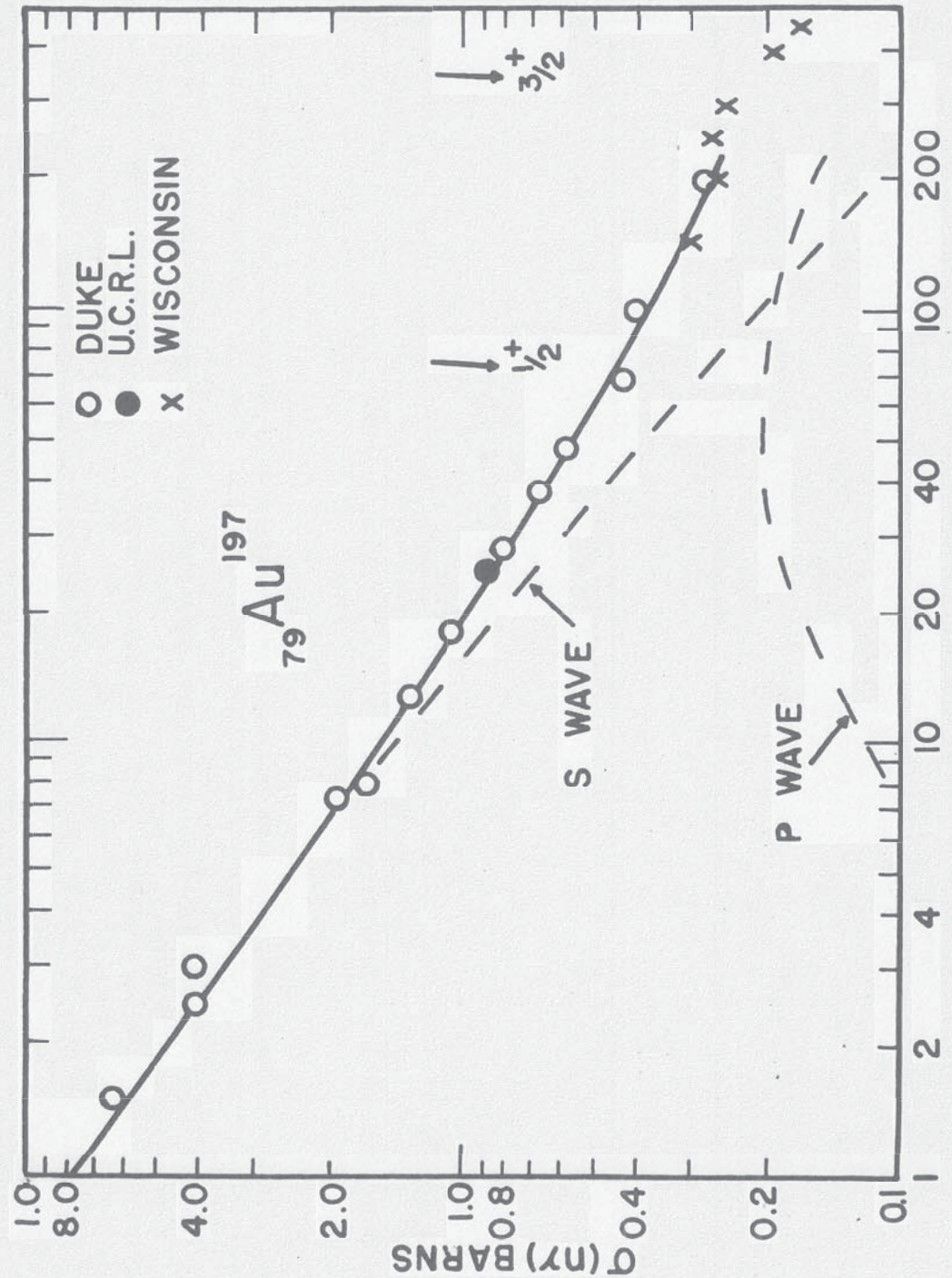
DUKE
U.C.R.L.
WISCONSIN
$^{197}_{79}Au$
$3^+/2$
$1^+/2$
S WAVE
P WAVE
σ (nγ) BARNS
En(KEV)
NEUTRON CAPTURE CROSS SECTION OF Au^{197}

Figure 13

capture cross sections; a similar break appears in the Pt^{196} curve which we were able to measure with very poor statistical accuracy because of its long half life and low isotopic abundance. We can not produce as sharp a break as is shown by the experimental data by incoherent addition of possible partial cross sections due to s- and p-wave neutrons. We are therefore forced to conclude that both p- and d-wave neutrons are responsible for the sharp rise in the capture cross section of Pt^{198} at forty kev. Since none of the resonance parameters are known for Pt and three different partial cross sections seem to be involved, we are unable to attempt a unique fit to the experimental data. It is interesting to note that a smooth extrapolation of the data in Figure 14 to higher energies tends to coincide with the absolute measured cross section at one Mev.[58]

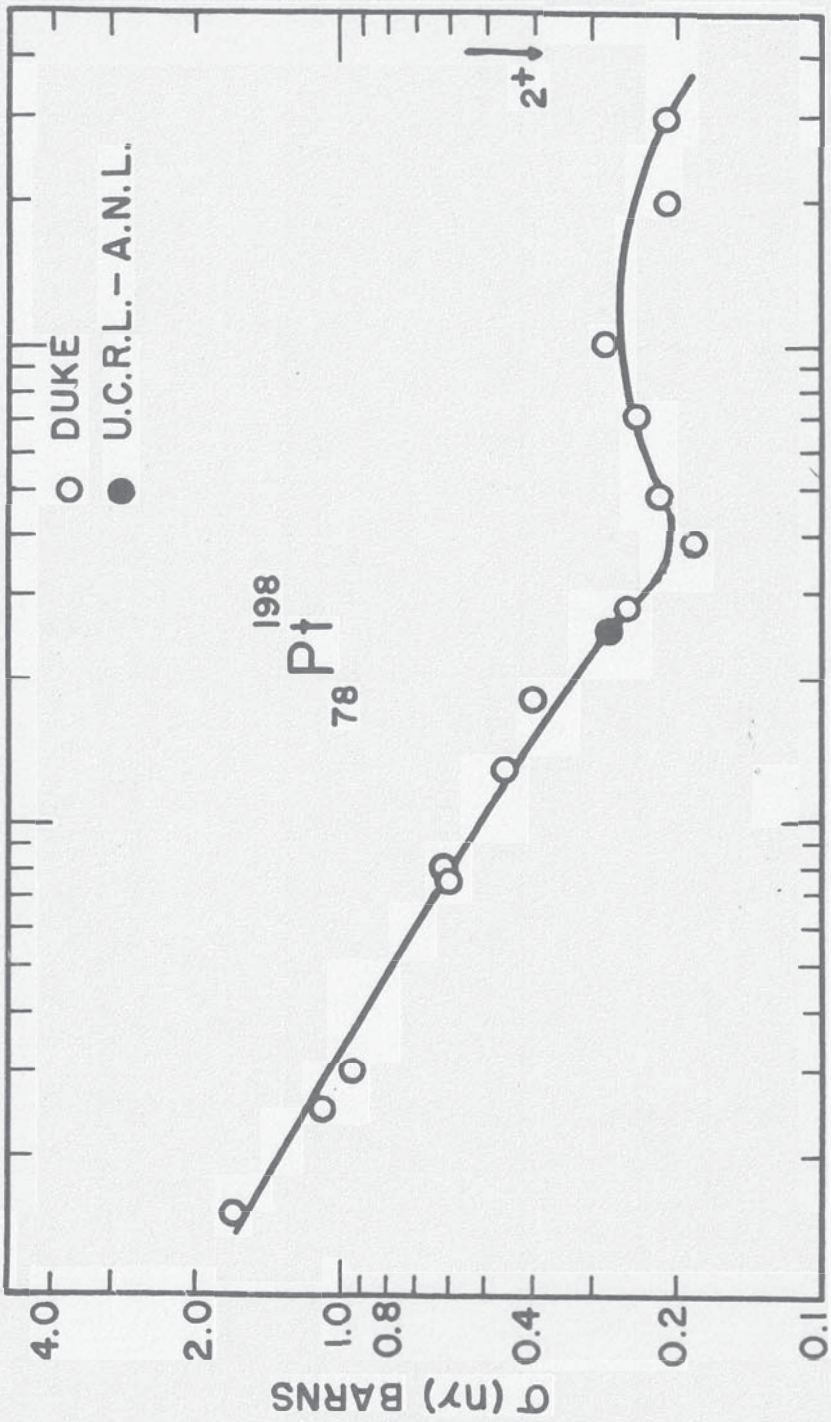
DUKE
U.C.R.L.-A.N.L.
$^{198}_{78}Pt$
2+
σ (nγ) BARNS
4.0
2.0
1.0
0.8
0.4
0.2
0.1
1
2
4
10
20
40
100
200
En(KEV)
NEUTRON CAPTURE CROSS SECTION OF Pt^{198}

Figure 14

Chapter IV

P-WAVE STRENGTH FUNCTIONS

Figure 15 shows p-wave strength functions as determined from the capture cross sections. Also included are results obtained by re-analysis of the experimental data of Newson et al.[11] according to the lines suggested in Chapter II. These include results for As, Se, Sr, Y, Zr.[90, 92, 94] The results for Sr*, Mo, Rh, Ag, Sn are obtained from the analysis of the unpublished data of Seth et al.[42] Also included are $\bar{\Gamma}_n^{(1)}/D$ for Niobium as measured by Bollinger et at.[59] and Rosen et al.[60] Preliminary values of the p-wave strength functions of Indium, Silver, and Niobium, as obtained from capture cross section measurements by Gibbons et al.[37] are in reasonable agreement with the above. For additional references

---

* Part of the Sr data used in this analysis is due to C. D. Bowman. See C. D. Bowman Master's Thesis, Duke University (1958).

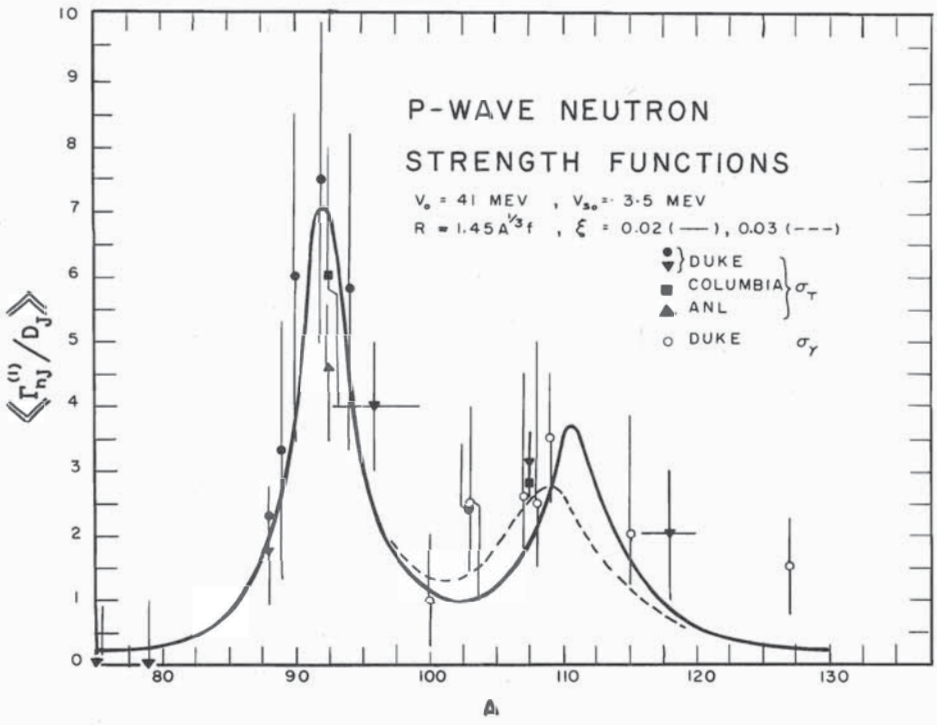
P-WAVE NEUTRON
STRENGTH FUNCTIONS
V_o = 41 MEV , V_{so} = 3·5 MEV
R = 1.45$A^{1/3}$f , ξ = 0.02 (——), 0.03 (---)
DUKE
COLUMBIA
ANL
σ_T
DUKE
σ_γ
$\langle\langle \Gamma^{(l)}_{nJ}/D_J \rangle\rangle$
A
0
1
2
3
4
5
6
7
8
9
10
80
90
100
110
120
130

FIGURE 15

see Table II, page 58.

The experimental results for p-wave strength functions are in disagreement with the predictions[3] of a simple square well optical potential:

$$V = V_o(1 + i\,\xi), \quad r \leq R \qquad (7)$$
$$V = 0, \quad r > R$$
$$\text{where } R = r_o A^{1/3}$$

The experimental p-wave strength functions indicate a much wider peak or peaks than the assumption of the above square well optical potential would produce. If we disregard the experimental evidence for the dip around $A \simeq 100$, a very large value of ξ would be required to produce so wide a giant resonance, and such a peak would have a maximum value of only about $\bar{\Gamma}_n^{(1)}/D = 2.0 \times 10^{-4}$; which is in obvious disagreement with the experimental data. Thus it is not possible to determine suitable parameters for the above optical potential which would reproduce the width as well as the height of the observed strength function peak.

The results for Mo^{100} and possibly Rh^{103} suggest that the distribution has a minimum or at least a plateau at $A \simeq 100$ and two peaks at $A \simeq 92$ and 110. The former has been reported previously.[11] Such a distribution would require that the results for two different VR^2 combinations giving peaks at $A \simeq 92$ and $A \simeq 110$ be superimposed. The two values of VR^2 at a given atomic weight can be obtained by requiring that either V or R be two-valued. In the region of A where spheroidal deformations of nuclei are expected, such a double peak in s-wave neutron

strength function (for which V must be single valued) has been explained by considering the two characteristic radii of a spheroid, i.e., considering R to be two-valued for a given A. In the region of atomic weights, A = 75 to 130, with which we are concerned, nuclei are known not to possess any large intrinsic quadrupole moments; thus V alone must be responsible for the double peak, i.e., it must be double-valued.

It is well known that high energy experiments indicate sizeable spin-orbit coupling in the nuclear interaction. Recent optical model analysis of neutron scattering[32] and proton scattering[61] data from four to four hundred Mev has shown that a definite spin-orbit potential must be included in the optical potential. At lower energy Okazaki[5] has deduced similar evidence from neutron polarization studies. The general optical potential for neutrons must therefore include a spin-orbit part and may be written as

$$V(r) = V_0(1+i\xi)\, f(r) + [\delta + i\gamma]\, V_0(\hbar/2mc)^2(2/r)(\partial f(r)/\partial r)(\underset{\sim}{s}\cdot\underset{\sim}{\ell}) \qquad (8)$$

if the same shape is assumed for real and imaginary parts of the potential. For a square well potential this yields a δ-function shape for the spin-orbit potential. However, Okazaki has shown that a suitable uniform spin-orbit potential can always be found which will reproduce the results of the δ-function potential. Further, below twenty Mev, Fernbach finds no evidence of the imaginary part of the spin-orbit potential. Thus we can write the simplified potential as:

$$V_{\pm} = -V_o \left[1+i\xi + \delta/2 \left\{ -1 \pm (2\ell+1) \right\} \right] , \quad r \leq R \qquad (9)$$

$$= 0 , \quad r > R$$

$$\bar{\Gamma}_n^{(\ell)}/D = (2\ell+1)^{-1} \sum_J g_J \left(\bar{\Gamma}_{nJ}^{(\ell)}/D_J \right) \qquad (10)$$

$$= (2\ell+1)^{-1} \left[(\ell+1) \langle \Gamma_{nJ}^{(\ell)}/D_J \rangle^{+} + \ell \langle \Gamma_{nJ}^{(\ell)}/D_J \rangle^{-} \right]$$

The solid curve in Figure 15 was obtained with the following choice of parameters: V_o = 41 Mev, ξ = 0.02, δ = 0.085 and R = 1.45 $A^{1/3}$ fermis and is found to fit the experimental data reasonably well. The dashed curve represents another possible fit with the parameters: V_o = 41 Mev, ξ = 0.30, and δ = 0.085. While no claim is made here that these are by any means the best fit parameters, it is to be noted that we have kept $V_o\bar{R}^2$ approximately the same as that chosen by Feshbach, Porter and Weisskopf[3] and our value of the spin-orbit potential = 3.5 Mev is in reasonable agreement with Okazaki's based on polarization studies. The fit at the minima near A = 102 and 130 might be improved by rounding off the nuclear potential.

It is felt that the experiments described have definitely shown that for p-wave neutrons there is an appreciable spin-orbit coupling term in the nuclear potential which brings about a splitting in the p-wave strength function peak predicted by the optical model at an atomic weight of about one hundred. Unfortunately, the evaluation of the p-wave strength functions was not sufficiently precise to determine the magnitude of the spin-orbit effect very accurately, but with improvement in experimental techniques and analysis this should be possible in the not too distant future. It was also found that for even-even nuclei the s- and p-wave γ-ray strength functions can differ by a

relatively large factor, and this fact can be explained qualitatively by considering parity effects in the shell model.

Table II

SUMMARY OF PARAMETERS

Target[a] Nucleus	Experiment	Known $\bar{\Gamma}_\gamma$ (ev)	Known $D_{obs.}$ (ev)	$(\bar{\Gamma}_\gamma/D_{obs.})_s$[b] Derived (units of 10^{-4})	$(\bar{\Gamma}_\gamma/D_{obs.})_s$[c] Used (units of 10^{-4})	$(\bar{\Gamma}_\gamma/D_o)_s$ (units of 10^{-4})	$\frac{(\bar{\Gamma}_\gamma/D_o)_p}{(\bar{\Gamma}_\gamma/D_o)_s}$
As^{75}	$\sigma_{n\gamma}$	0.287	100[8]	28.7	66.0	8.25	≤ 1.0
Mo^{100}	$\sigma_{n\gamma}$	0.260	~500[34,15]	~5.2	2.0	1.0	≤ 1.0
Rh^{103}	$\sigma_{n\gamma}$	0.155	~20[d ,15]	~77.5	Not Unique	----	~1.0
Ag^{107}	$\sigma_{n\gamma}$	0.130 0.130 0.137	25[47] 19[48] 34[49]	52.0 68.0 40.0	100.0	25.0	0.75±0.3
$Ag^{107,88}$	σ_T	----	----	----	50.0	12.5	----
Pd^{108}	$\sigma_{n\gamma}$	----	----	----	60.0	30.0	0.4 ± 0.3
Ag^{109}	$\sigma_{n\gamma}$	0.134 0.130 0.137	17[48] 16.5[47] 19[49]	78.8 78.8 71.0	---- 79.0 ----	---- 19.8 ----	---- 1.0 ± 0.3 ----
In^{115}	$\sigma_{n\gamma}$	0.077	7[34]	110.0	120.0	6.0	1.0 ± 0.3
Au^{197}	$\sigma_{n\gamma}$	0.125	25[15]	50.0	180.0	26.6	1.0 ± 0.3
Pt^{198}	$\sigma_{n\gamma}$	0.095	(?)	----	Not Unique	----	----
U^{238}	$\sigma_{n\gamma}$	0.023	19[34]	12.7	13.0	6.5	2.6 ± 0.5

TABLE II (Continued)

Target[a] Nucleus	Experiment	R' used (units of 10^{-13}cm)	$(\bar{\Gamma}_n^{(0)}/D)$ used (units of 10^{-4})	$(\bar{\Gamma}_n^{(1)}/D)$ obtained[e] (units of 10^{-4})
As^{75}	σ_T	8.0 ± 0.5[12]	1.83 ± 0.7[8] 2.50 ± 0.5[9]	≤ 1.0
As^{75}	$\sigma_{n\gamma}$	----------	----------	Not unique
$Se^{78.96}$	σ_T	7.5 ± 1.0[f]	2.43 ± 1.0[g]	< 1.0[h]
$Sr^{87.63}$	σ_T	6.7[i]	0.54[j]	$2.0 \pm {}^{0.75}_{1.00}$
$Y^{88.92}$	σ_T	6.7 ± 0.1[f]	0.50 ± 0.4[g]	3.3 ± 2.0
Zr^{90}	σ_T	7.1 ± 0.2[f]	0.54[j]	6.1 ± 2.4
$Zr^{91.32}$	σ_T	----------	----------	7.5[k]
Zr^{92}	σ_T	7.1 ± 0.2[f]	0.54[j]	7.5 ± 2.5
Nb^{93}	σ_T	----------	----------	6.0 ± 2.0[60]
Nb^{93}	σ_T	----------	----------	4.5 ± 1.0[50]
Zr^{94}	σ_T	7.1 ± 0.2[f]	0.54[j]	5.8 ± 2.4
$Mo^{95.95}$	σ_T	6.8 ± 0.1[f]	0.38 ± 0.11[11]	4.0 ± 1.0
Mo^{100}	$\sigma_{n\gamma}$	----------	0.50[j]	1.0 ± 1.0
$Rh^{102.91}$	σ_T	6.6 ± 0.6[d]	0.50[j]	2.4 ± 1.0

TABLE II (Continued)

Target[a] Nucleus	Experiment	R' used (units of 10^{-13} cm)	$(\bar{\Gamma}_n^{(0)}/D)$ used (units of 10^{-4})	$(\bar{\Gamma}_n^{(1)}/D)$ obtained[e] (units of 10^{-4})
Rh^{103}	$\sigma_{n\gamma}$	----------	0.50 [j]	2.4 ± 1.5
Ag^{107}	$\sigma_{n\gamma}$	----------	0.50 ± 0.2 [10]	$2.6 \pm {}^{1.9}_{0.8}$
$Ag^{107.88}$	σ_T	6.7 ± 0.2 [f]	0.53 ± 0.1 [50]	3.1 ± 0.4
Pd^{108}	$\sigma_{n\gamma}$	----------	0.50 [j]	$2.5 \pm {}^{4.5}_{1.0}$
Ag^{109}	$\sigma_{n\gamma}$	----------	1.00 ± 0.3 [10]	3.3 ± 1.0
In^{115}	$\sigma_{n\gamma}$	----------	0.31 ± 0.06 [10]	$2.0 \pm {}^{2.6}_{0.8}$
Au^{197}	$\sigma_{n\gamma}$	----------	1.20 ± 0.30 [10]	0.33 ± 0.3
Pt^{198}	$\sigma_{n\gamma}$	----------	[?]	Not unique
U^{238}	$\sigma_{n\gamma}$	----------	1.15 ± 0.15 [10] 0.95 ± 0.06 [m]	0.7 ± 0.3

a. Fractional atomic weights indicate natural elements.

b. Compare these values with those in the next column.

c. No values of $(\bar{\Gamma}_\gamma/D_{obs.})_s$ used in analysis are listed for total cross section experiments other than natural silver because the relation, $(\bar{\Gamma}_n/D) \gg (\bar{\Gamma}_\gamma/D_J)$ made the effect of this parameter negligible.

d. V. L. Sailor, Phys. Rev. 91, 53 (1953).

e. The final errors indicated include the contributions due to our experimental errors, possible errors in absolute normalization, and our estimate of uncertainty due to the non-uniqueness of the method of analysis.

f. K. K. Seth, D. J. Hughes, R. L. Zimmerman, and R. C. Garth, Phys. Rev. 110, 692 (1958).

g. J. M. LeBlanc, R. E. Cote, and L. M. Bollinger, Nucl. Phys. 14, 120 (1959).

h. F. Boreli and S. E. Darden (Phys. Rev. 109, 2079, 1958) obtain a value of $\bar{\Gamma}_n^{(1)}/D = 3.04 \times 10^{-4}$ for Se. The discrepancy is supposedly due to their use of $\bar{\Gamma}_n^{(0)}/D = 0.88 \times 10^{-4}$, a value much smaller than that reported by LeBlanc[g].

i. Calculated from unpublished data in BNL-325[15].

j. Interpolated best values from a plot of experimentally known (unpublished) values and the optical model predictions.

k. F. Boreli and S. F. Darden, Phys, Rev. 109, 2079 (1958).

l. J. L. Rosen, CU-185, Ph.D. Thesis, Columbia University (1959).

APPENDIXES

Appendix I

AVERAGE TARGET THICKNESS

Since the measurement of average capture cross sections required only very modest neutron energy resolution, targets used for the production of neutrons with the Van de Graaff proton beam could be thick compared to those necessary for higher resolution work. Even at the lowest neutron energies used in these measurements, the effect on resolution due to a target of the order of two kev proton stopping power was small compared to the energy spread due to the angular acceptance of the sample. Above fifty kev, targets of the order of ten kev stopping power could be used. Even though target thickness had a negligible effect on the resolution with which the measurements were made, the average thickness of the target was important in determining the nominal energy of the neutron beam.

Estimating the average target thickness from forward threshold (in terms of proton stopping power) has long been the common procedure in neutron spectroscopy. This method had not been developed into an accurate procedure, since previously the method had been used extensively only to ascertain that the target was very thin. When an estimate of the thickness of a relatively thick target was necessary, it was generally assumed that the

proton stopping power was the energy interval between forward threshold energy and the energy at which the yield of neutrons at zero degrees started decreasing. This method was of doubtful accuracy because thin layers of lithium fluoride, of which a target consists, are known not to be of uniform thickness. A program was carried out to find a better method of interpreting forward threshold measurements in terms of average target thickness.

The total cross section and the total neutron yield just above forward threshold of the Li(p,n) reaction has been studied in detail by Newson and Williamson[62] and by Gibbons et al.[63] It was found that a broad $2^-(\ell = 0)$ resonance at approximately 1.9 Mev accounts for almost all the observed neutron yield from threshold to about 1.95 Mev. This cross section can be expressed in the form:

$$\sigma_{pn} = 4\pi \lambda\!\!\!^{-2} g_J \, X/(1+X)^2 \qquad (11)$$

where $\lambda\!\!\!^{-}$ = DeBroglie wave length of incident protons.

$g_J = (2J + 1)/2(2I + 1)$

$X = \Gamma_n / \Gamma_p = C\,[(E_p - E_t)/E_p]^{1/2}$ = ratio of the neutron and proton partial widths of the resonance.

E_t = neutron threshold of Li(p,n) reaction.

Newson et al. found the constant C = 6 fitted the data with reasonable accuracy while Macklin and Gibbons determined the value $C = 5.2 \pm 0.3$. The constant, C, is difficult to determine accurately by means of total yield or total cross section measurements since forward threshold energy must be determined by the same data.

The above equation was used to calculate the differential cross section of the Li(p,n) reaction at zero degrees up to about fifty kev above forward threshold. Since the resonance dominating the cross section in this energy range was an s-wave resonance, the reaction was assumed to be isotropic in the center of mass system. With the above assumption, geometrical considerations led to the following expression for the differential cross section at zero degrees:

$$\sigma_{pn}^{(\theta \simeq 0)} = \sigma_{pn} \left\{ 1 - 0.5 \left(1 - \left[1 + (y^2 - \theta^2)^{1/2} \right]^2 \theta^2 / y^2 \right)^{1/2} - 0.5 \left(1 - \left[1 - (y^2 - \theta^2)^{1/2} \right]^2 \theta^2 / y^2 \right)^{1/2} \right\} 1/\Delta\Omega \quad (12)$$

where $\Delta\Omega$ = small solid angle subtended about zero degrees.

θ = polar angle defining $\Delta\Omega$.

$y = 7 \left[(E_p - E_t)/E_p \right]^{1/2}$

The above expression is valid only for small θ such that the approximation $\sin\theta \simeq \theta$ and $\cos\theta \simeq 1$ can be made. Also the equation does not apply when $y < \theta$. This condition occurs slightly above threshold (about one hundred ev for $\theta = 0.051$ rad) where all the neutron yield from the reaction is contained within $\Delta\Omega$.

At back threshold (proton energy at which neutrons emerge into angles greater than ninety degrees) the last major term in equation 12 goes to zero and should be ignored at higher proton energies. This is due to the fact that the center of mass velocity towards zero degrees is no longer greater than that of a neutron emitted at an angle of 180° in the center of mass and the lower energy neutron group is no longer present at the forward angles.

At proton energies greater than about four kev above forward threshold, the expression for the differential cross section for the Li(p,n) reaction (equation 12) can be approximated by the following expression within ± 2 percent:

$$\sigma_{pn}(\theta \simeq 0) \cong \sigma_{pn}\left[(1 + y^2)/y^2\right] \theta^2/(2\Delta\Omega) \qquad (13)$$

Therefore, in the energy region where this approximation is valid, there is not a strong dependence on θ, $(\Delta\Omega \propto \theta^2)$, and the finite solid angle which a counter subtends has a smaller effect on an experimental measurement.

The differential cross section is experimentally measurable only with a target which has negligible stopping power for protons. Even an approximate experimental measurement of such a cross section is very difficult near forward threshold where the cross section is rapidly varying. The validity of the calculated differential cross section could be determined with the use of a very thick target (stopping power greater than $E_p - E_t$), i.e., a measurement of what should be the energy integral of the differential cross section from threshold to the proton energy. Such a measurement has the advantage that the roughness of the target layer has no appreciable effect on the yield so long as there are no bare spots and there are no impurities in the lithium or lithium compound. This is due to the fact that protons which are above forward threshold all penetrate about the same number of lithium atoms per square centimenter per kev energy loss. Such a thick target threshold would be affected by the proton beam resolution and proton straggling but these effects are appreciable only for the first few kev.

A forward threshold taken with the McKibben counter and a very thick lithium fluoride target is shown in Figure 16. Lithium fluoride was used instead of lithium since a lithium metal target deteriorates upon exposure to air and may not have an equal number of lithium atoms per kev energy loss for protons. The proton resolution was 1/2000 for the measurement of this threshold. The experimental data is normalized to the solid line which is the integral of the differential cross section from threshold to the energy plotted. A triangular resolution of 1/2000 was folded into the calculated curve to take account of the spread in the proton energy. Integration of the differential cross section was done by integrating equation 12 numerically up to an energy of four kev; equation 13 was integrated analytically above this energy. At thirty seven inches from the target the McKibben was assumed to have an active counting radius which subtended an angle of 0.051 radians. This assumption had little effect on the shape of the calculated curve. Comparison of the shapes of the calculated and experimental thick target threshold curves shows that the assumptions used to derive the differential cross section seem to be valid to a good approximation. It has been shown with a BF_3 counter that our McKibben counter has a flat response over the neutron energy region covered by this thick target threshold curve (see Chapter I, Monitors).

From the normalization required to match the experimental data in Figure 16 with the calculated curve, it was possible to calculate the efficiency of the McKibben counter. Since the

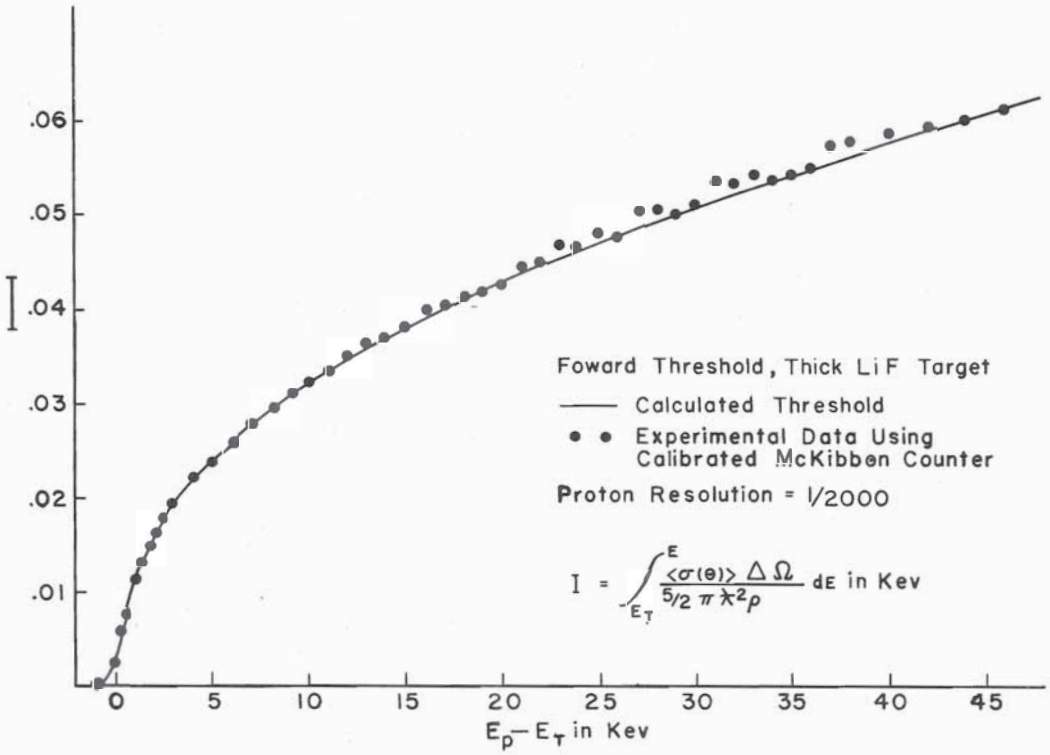
.06
.05
.04
.03
.02
.01
I
0
5
10
15
20
25
30
35
40
45
$E_p - E_T$ in Kev
Foward Threshold, Thick LiF Target
Calculated Threshold
Experimental Data Using Calibrated McKibben Counter
Proton Resolution = 1/2000
$I = \int_{E_T}^{E} \frac{\langle\sigma(\theta)\rangle \Delta\Omega}{5/2\,\pi\lambda^2\rho} d\varepsilon$ in Kev

FIGURE 16

calculated differential cross section was dependent on θ^2 above four kev, this efficiency could best be determined in terms of the neutron flux at the face of the McKibben counter and the McKibben counting rate. Using the constant, C = 6, as determined by Newson et al.,[62] the stopping power for protons of lithium and fluorine,[64] and the fact that the McKibben was thirty seven inches from the target, the following relation was derived:

$$0.45\ R = \Phi \qquad (14)$$

where R is the counting rate of the McKibben at a distance of thirty seven inches from the target and Φ is the neutron flux at the same position.

The above result is in good agreement with two other experimental measurements. Using the hydrogen recoil counter described in Appendix II as an absolute neutron flux monitor, the result $0.42\ R = \Phi$ was obtained. This measurement was done at neutron energies of from 100 to 650 kev, but since the efficiency of the McKibben counter is supposedly flat in the kev region, the energy difference should not be important. The other measurement of this type was done by E. G. Bilpuch using a calibrated neutron source. This neutron source was a three curie, antimony-beryllium source which was borrowed from Oak Ridge National Laboratory (calibrated by the National Bureau of Standards). The neutrons emitted had an average energy of about twenty five kev with an energy spread of plus or minus a few kev. By placing the McKibben counter the standard thirty seven inches from this source, the relation $0.48\ R = \Phi$ was obtained. It

should be noted that the results of both these experiments are in good agreement (± 6 percent) with equation 14 which was based upon the differential cross section of the Li(p,n) reaction. These calibrations, of course, assume the use of the same BF_3 counter (one inch in diameter, six inches long, and filled with enriched $B^{10}F_3$ at a pressure of fifty cm of Hg) in the McKibben.

Since the integral of equation 12 was justified by thick target thresholds, it was possible to interpret forward threshold curves of targets which were of a thickness useful for the relative capture cross section measurements. From the calculated thick target threshold curve, an ideal forward threshold curve for a uniform target of finite thickness is easily derived. Each increment of a target may be considered as an independent contributor to the threshold curve since, to a good approximation, protons lose energy linearly as they proceed through a target which is not too thick. Thus, an ideal forward threshold curve for a relatively thin target can be produced by displacing the calculated thick target threshold curve by the stoping power of the target thickness desired and subtracting this curve from the original calculated thick target threshold curve.

The experimental forward threshold curve for a LiF target of 1.6 kev average stopping power is shown in Figure 17. The solid curve is the calculated forward threshold curve (for a 1.6 kev stopping power target) which best fit the experimental data. This calculated curve belonged to a family of calculated curves, corresponding to a variety of target thicknesses, which were used to determine target thickness by a method to be described.

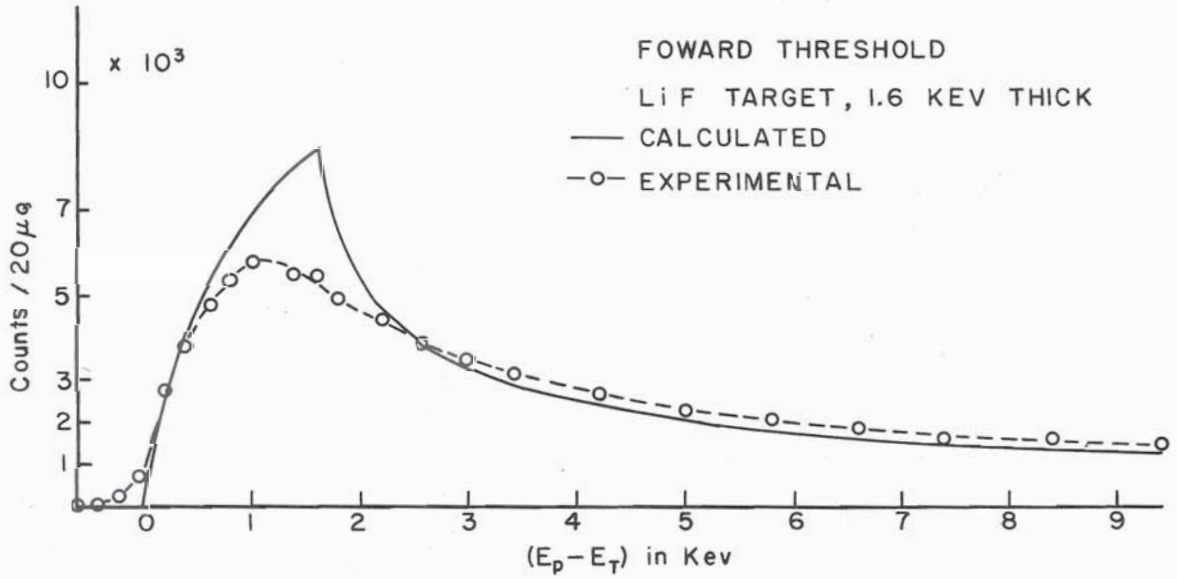
FOWARD THRESHOLD
LiF TARGET, 1.6 KEV THICK
CALCULATED
EXPERIMENTAL
x 10³
Counts / 20μq
10
7
5
3
2
1
0
1
2
3
4
5
6
7
8
9
(Ep − ET) in Kev

FIGURE 17'

We attribute the deviation of the experimental data from the calculated curve to the roughness of the LiF target, proton straggling, and the proton resolution. The calculated and experimental threshold curves do not reach agreement until far above threshold energy. For the case shown, the curves do not match until about 25 kev above threshold energy. Thus the effect of roughness of the target is quite large near forward threshold because the differential cross section is such a strongly peaked function near forward threshold energy.

The method of fitting a forward threshold curve for a relatively thin target with a calculated curve (in order to find the average thickness of the target) involves the fact that the two curves should join at the extrapolated forward threshold as well as at an energy far from forward threshold and that the area under the experimental and calculated curve should be the same. The first two conditions are usually sufficient, however, the third is usually a good check and improves the accuracy of the result. Under the experimental conditions used, the normalization between the calculated curve and the experimental threshold could be determined with the use of a thick target threshold by the method already described (see Figure 16, page 68). At this laboratory, forward threshold curves are usually taken with the use of a proton charge integrator so that the number of McKibben counts for so many microcoulombs of proton charge are recorded at each proton energy. Since it was possible to normalize the calculated threshold curve to a certain number of microcoulombs (usually twenty), a family of forward threshold

curves for various target thicknesses was calculated to correspond to the possible experimental data. By plotting the experimental threshold curve on the same scales, and matching the forward threshold energies it was possible to determine the average target thickness by observing which of the high energy asymptotes of the calculated curves the experimental data joined. Usually this result was checked by determining whether the area of the two curves was the same. This procedure was thought advisable since the calibration of the McKibben counter was not checked by taking a thick target forward threshold before each target thickness determination. If for some reason the efficiency of the McKibben counter had changed, then a discrepancy in the areas of the calculated and experimental curves would have appeared. The above method of determining average target thicknesses is only applicable when the target is composed of a pure lithium compound or uncontaminated lithium metal.

Results of the study of target thicknesses indicated that the peak yield in a threshold curve was not always a good indication of the average target thickness. In every case it was found that the average target thickness was somewhat greater than the energy from forward threshold to the peak of the neutron yield; how much greater depended on the roughness of the target, which seemed to vary considerably. The reason for this effect is believed to be that the differential cross section of the Li(p,n) reaction is peaked just above forward threshold and thus the neutron yield from a target will drop as soon as appreciable numbers of protons penetrate the far side of the target

with energies above forward threshold. This drop in yield would indicate the exact target thickness only if the target were uniform, however, target layers are known not to be uniform and there is usually an appreciable quantity of target material which is outside the minimum thickness of the target.

The degree of roughness of a target was found to be determined to a large extent by the vacuum under which the target was evaporated. If the pressure exceeded about 0.5×10^{-4} mm of mercury during evaporation, it was found that the resulting target was very rough, and thus would cause an unnecessarily large resolution spread if used.

Lithium fluoride targets did not show any appreciable deterioration in air, while lithium metal targets apparently became rougher as well as thicker (due to LiOH formation) when exposed to the atmosphere. This alone, however, would not make such targets inferior to LiF targets, since after exposure, lithium targets have a stopping power within a few percent of that of a lithium fluoride target which produces the same neutron yield. The fact that the lithium targets appear to become rougher if the target is exposed to air makes lithium fluoride targets more desirable under many circumstances.

The experimental arrangement for the measurement of relative capture cross sections was such that targets had to be evaporated in an external evaporator and thus exposure to air was necessary. Due to this fact, it was thought necessary to study average target thicknesses in the manner which has been described. Several of the capture cross section curves which had originally

been done using thin lithium metal targets were repeated at the lower energies (less than fifty kev) with LiF targets of average target thickness determined by the methods described in this appendix. It was found that early empirical interpretations of the average thickness of the lithium metal targets were valid in most cases to within the accuracy necessary for the capture cross section measurements. Such empirical interpretations of forward thresholds were not consistent, however, in certain cases where the lithium metal targets were very rough.

During the activation measurements the McKibben counter was situated at ninety degrees with respect to the proton beam. Periodically it was necessary to check whether the target had been damaged during use. Since it was not desirable to move the McKibben during the activation measurements, another method of observing the condition of the target was devised. The small BF_3 counter used as a monitor below twenty five kev was used for this purpose. This counter had a response which decreased as $1/E_n^{1/2}$. It can be shown that the ninety degree neutron yield, just above back threshold, from a lithium target of relatively low stopping power rises approximately as $E_n^{1/2}$ after the protons penetrate the far side of the target with an energy greater than that of back threshold. Thus a back threshold curve taken with the BF_3 counter rose approximately linearly until the far side of the target was penetrated by protons of energy greater than back threshold and then the back threshold curve had a broad plateau. Such a ninety degree threshold curve taken with the BF_3 counter (1.2 inches from the center of the target to the

mid-point of the axis of the counter) is shown in Figure 18. By measuring such a back threshold curve at the start of the activation measurements and at later intervals, the condition of the target was known at all times since changes in the back threshold curve were easily interpreted. Back threshold measurements were also a good check on the thickness and roughness of the target as determined by the other methods described.

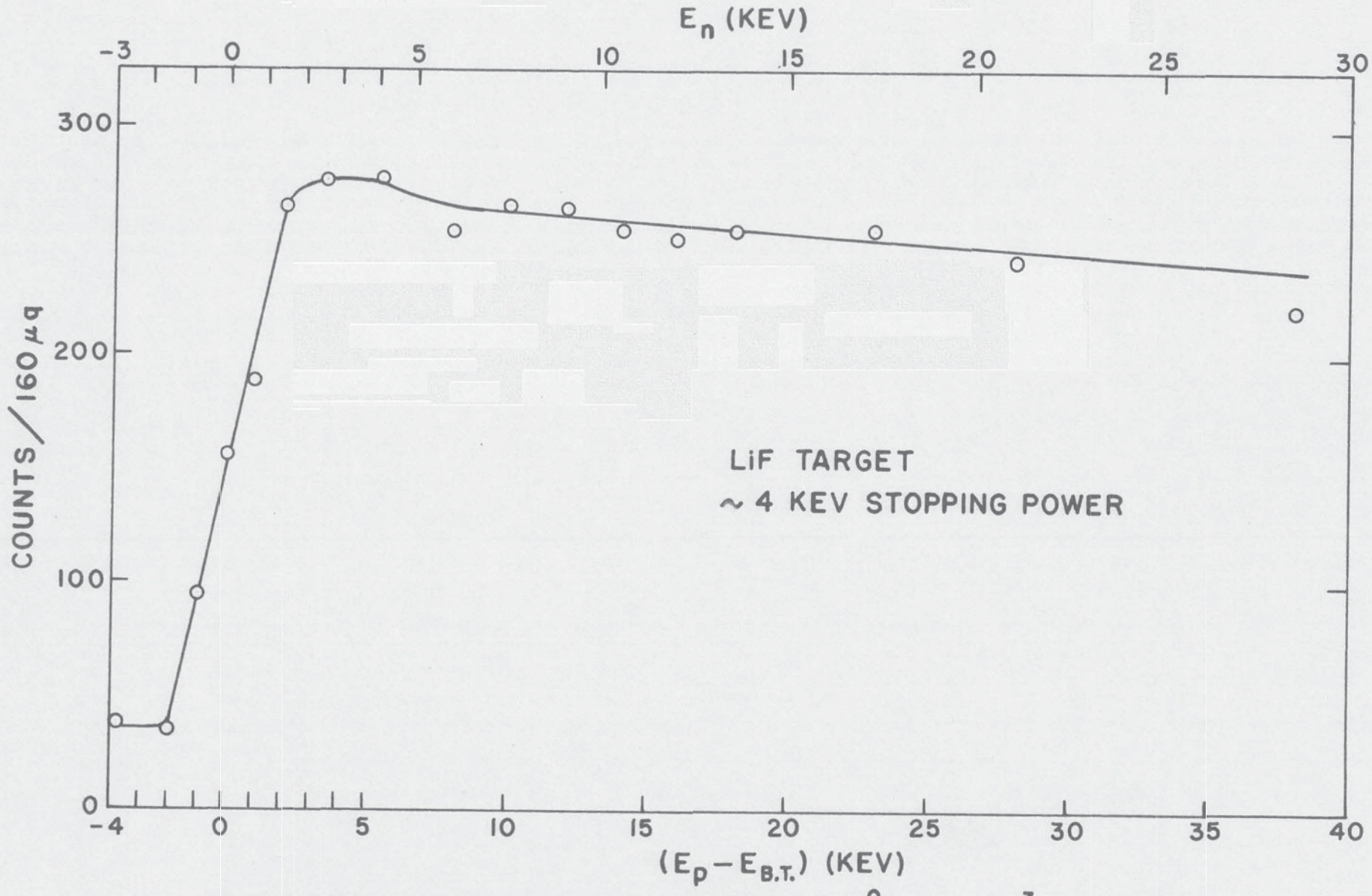

NEUTRON BACK THRESHOLD CURVE AT 90° WITH BF^3 COUNTER

Figure 18

Appendix II

HYDROGEN RECOIL COUNTER

A hydrogen recoil counter was constructed for the purpose of measuring the relative efficiency of the McKibben counter over as large a neutron energy range as possible (up to about 650 kev). The recoil counter was not used directly as a neutron monitor in the capture cross section experiments since its counting rate was low, compared to the McKibben counter, and background corrections were more difficult.

A recoil counter patterned after that of Allen and Ferguson[65] was constructed with only minor structural changes which made it feasible to build the counter in the Duke University Instrument Shop. A scale drawing is given in Figure 19. Structural materials were kept to a minimum to avoid unnecessary neutron scattering. The outer wall of the counter was designed to be at ground potential and formed no part of the active counting volume. This outer wall was capable of being evacuated and should have been able to withstand a maximum internal pressure of two atmospheres. The center wire of the counter was of 0.004 inch platinum wire and was thoroughly cleaned and inspected under a microscope to insure uniformity. The center wire was supported at both ends by kovar seals which acted as insulators; the external kovar seal

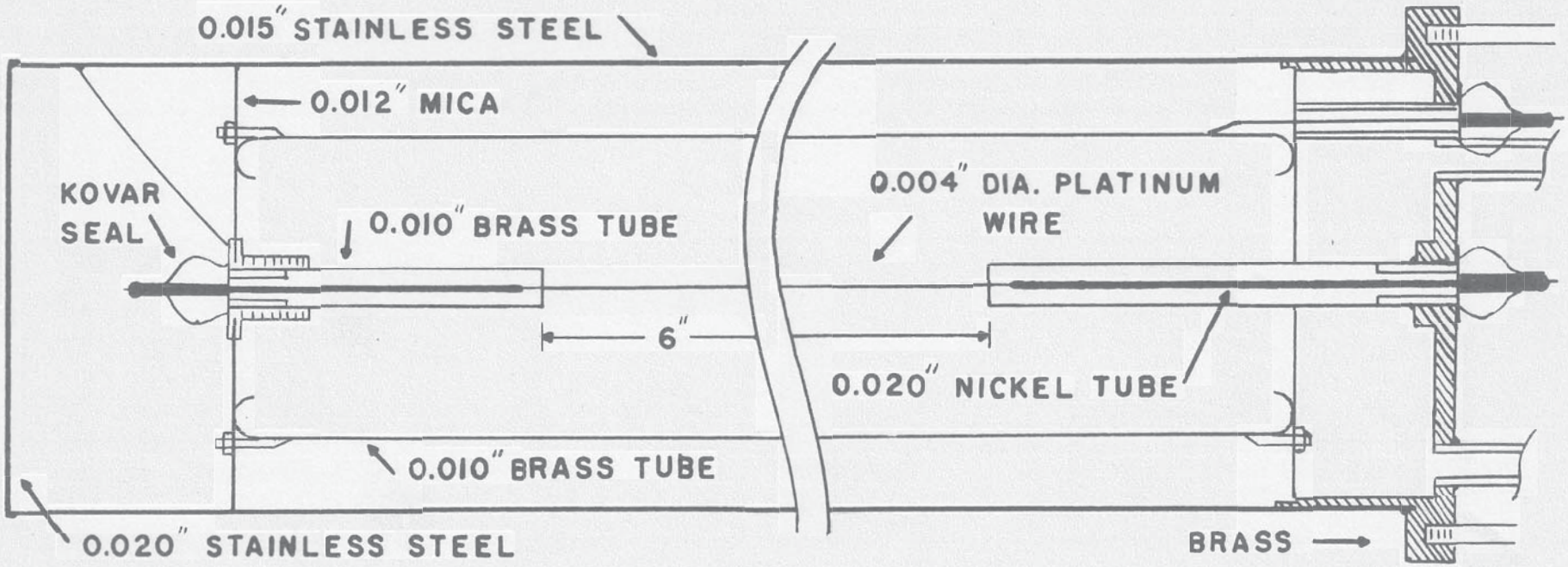

HYDROGEN RECOIL COUNTER

Figure 19

(see Figure 19) was used as the positive voltage terminal. In order to assure a uniform, radial electric field around the center wire, it was necessary to restrict the counting volume with the 0.25 inch diameter, brass field tubes which surround the center wire at both ends of the counting volume. These field tubes were grounded to the outer wall of the counter. Inside the field tubes, the center wire was surrounded by 0.020 inch diameter nickel tubing to prevent pulses originating between the center wire and the field tubes. The inner field tube and kovar seal were soldered to a stainless steel nut which secured this assembly to the mica support; the latter also supported the 1.81 inch brass cylinder which formed the cathode of the counter. The ends of this brass cylinder were rolled under to further assure a uniform field to the center wire and to prevent high voltage arcs. The other end of the brass cylinder was also secured to a mica support, and a voltage lead was brought out from the cylinder through a kovar seal so that it could be at a negative potential with respect to the field tubes and center wire. Thus, the active counting volume of the counter was defined by the inner ends of the field tubes and the inner surface of the 1.81 inch diameter brass cylinder which acted as the cathode.

The center wire of the counter was designed to be at a high positive potential, the field tubes at ground potential and the brass cylinder at a negative potential. The ratio of these two voltages was fixed by the condition that the field tubes must lie on a zero potential surface in order not to distort the electric field between the center wire and the cathode. For the

particular counter constructed, the ratio of positive to negative voltages should be 2.1. As long as this condition was satisfied to within the order of ten percent, the recoil counter was found to operate satisfactorily. It was necessary to mount a preamplifier directly behind the counter since the additional capacitance of coaxial cables decreased the pulse heights significantly.

A recoil counter as shown in Figure 19 should be capable of measuring an absolute flux of monoenergetic neutrons in the energy range of from about thirty kev to one Mev. However, such a neutron energy range cannot be covered without changing the operating conditions of the recoil counter. Ion multiplication, observed pulse height, and end effect corrections decrease with increasing gas pressure for constant high voltage on the counter. In a given energy range a compromise must be made among the above factors since a given counter can sustain a limited high voltage without breakdown. It was found that the counter yielded suitable pulse height spectrums for neutrons in the energy range of from 100 to 650 kev when filled with one atmosphere of hydrogen.

Figure 20 shows a differential pulse height spectrum for neutrons of two hundred kev average neutron energy from a lithium target which had a proton stopping power of approximately twenty kev. This spectrum was taken with 1,900 volts on the center wire and one atmosphere of hydrogen in the counter. An ideal pulse height spectrum would be one in which all pulse heights up to that corresponding to the maximum neutron energy were equally probable, and then have a sharp cut off. Two effects

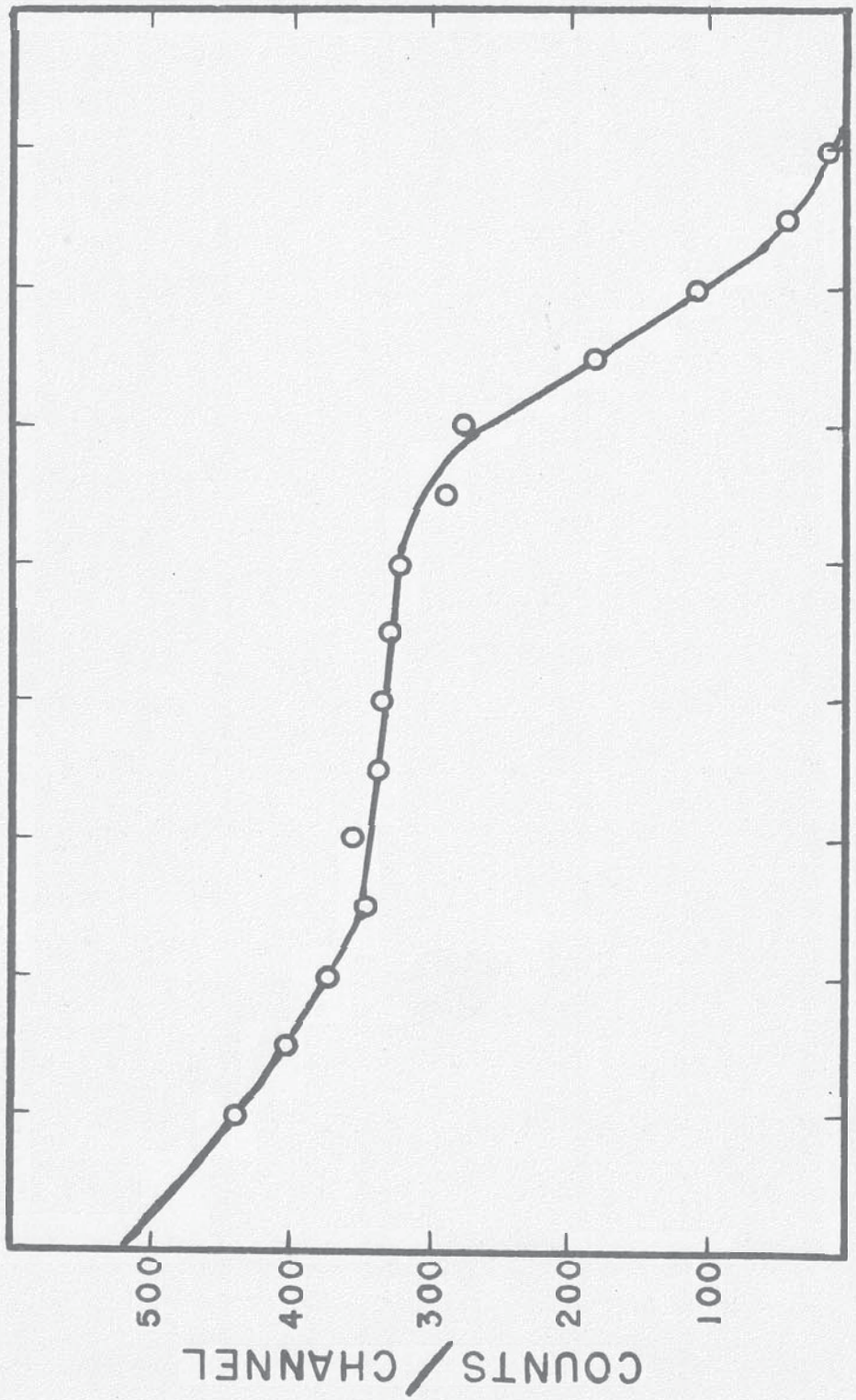
COUNTS / CHANNEL
500
400
300
200
100
2
4
6
8
10
12
14
16
PULSE HEIGHT (VOLTS)
DIFFERENTIAL RECOIL SPECTRUM OF 200 KeV. NEUTRONS

Figure 20

make such a spectrum impossible to attain: (a) impurities in the gas, and (b) recoil protons either entering or leaving the active counting volume (or hitting the cathode wall) before they have lost all their energy by ionizing collisions with hydrogen molecules. Both the above factors cause the pulse height cut off to be less distinct and the spectrum not to be flat up to cut off.

Hydrogen must be very pure in order to be suitable for use in a hydrogen recoil counter. Impurities usually have very different neutron cross sections and ionization properties from those of hydrogen, and thus change the pulse height spectrum and destroy the accuracy of an absolute flux calibration. The recoil counter was provided with two gas inlets as can be seen in Figure 19, page 79. This was done in case it were necessary to build a constant flow gas purifier for the counter. Such a procedure was not carried out since it was found that Research Grade Hydrogen provided by Matheson Company was pure enough for our purposes. A metal filling system with diffusion pump, dry ice trap and liquid air trap was constructed for filling the counter with hydrogen. The evacuated counter and filling system were heated to a temperature of about 100° C several times before filling the counter in order to minimize outgassing of the metal parts during or after the filling of the counter. Heating to a higher temperature was not possible because of several soft solder joints in the counter. Outgassing of the counter after filling was evidently not very serious since the quality of the experimental pulse height spectra did not deteriorate noticeably

over a period of several weeks.

Neutron flux could be measured with the counter described above by placing the counter axis parallel on the neutron beam and recording the pulse height on a multi-channel analyzer. It is easily seen that the area under the differential pulse height spectrum is proportional to the neutron flux to which the counter is exposed if corrections are made for end effects and for the variation of the neutron-proton scattering cross section with neutron energy. A differential pulse height spectrum is taken instead of an integral count since it is necessary to extrapolate the pulse height spectrum back to zero pulse height in order to eliminate electrical noise. An integral count would have been sufficient if the recoil spectra were very close to ideal, so that the count could have been biased above all electrical noise and it could have been assumed that the spectrum was flat below this bias.

The neutron flux is related to the area under the differential pulse height spectrum in the following manner:

$$A(\text{counts/sec}) = n\,\sigma(E_o)\,N(E_o)\,\bar{\Phi} \qquad (15)$$

where A = area under pulse height spectrum per second.

n = atoms of hydrogen contained by the active counting volume.

$\sigma(E_o)$ = neutron-proton scattering cross section for neutrons of E_o energy.

$N(E_o)$ = end effects correction.

$\bar{\Phi}$ = neutron flux of E_o energy.

For the particular counter constructed, the above relation re-

duces to:

$$\Phi = 7.33\ (p/76)\ A/(\sigma N) \qquad (16)$$

where p is the pressure in centimeters of mercury, and σ is in barns.

The neutron scattering cross section of hydrogen has been measured to one hundred kev by Masket.[14] These measurements are in excellent agreement with theoretical calculations in BNL-325.[15] Since the recoil counter was used at energies up to 650 kev, the values of $\sigma(E_o)$ above one hundred kev were taken from the theoretical calculations mentioned above.

The end effects correction, $N(E_o)$, for a recoil counter has been considered in detail by Skyrme, Tunnicliffe, and Ward,[66] and Allen and Ferguson.[65] Such corrections are necessary because some of the recoil protons enter or leave the active counting volume (or strike the cathode wall) before they have lost all of their energy. These corrections depend upon the radius and length of the counter as well as on the neutron energy, i.e., the average effective range of protons in hydrogen. Using the appropriate integrals evaluated by Skyrme et al.,[66] and dE/dX for protons in hydrogen as measured by Weyl,[67] $N(E_o)$ was calculated to be 1.042, 1.092, and 1.33 for neutron energies of 250, 500, and 1000 kev respectively when the recoil counter is filled with one atmosphere of hydrogen.

The experiment in which the recoil counter was used (measuring the relative efficiency of the McKibben counter) was carried out using neutrons at zero degrees from a twenty kev stopping power lithium target. With this experimental arrangement, the

measurements could not be extended below one hundred kev because of the low energy group of neutrons emitted by the target at these lower nominal energies. The recoil counter (12.31 inches effective distance from the target) and the McKibben counter (57 inches from the target) were placed so that they subtended the same effective solid angle, thus the recoil counter was between the target and the McKibben counter. The recoil counter was removed when a count was being taken by the McKibben. A proton charge integrator was used to assure that the recoil counter and the McKibben counter were exposed to the same number of neutrons per square centimeter. The reproducability of this procedure was found to be about $\pm$ 2 percent, which was within the desired experimental accuracy. The use of zero degrees for this experiment had two advantages: background due to scattered neutrons was negligible and the positioning of the two counters was much less critical. The results of the above experiment have been discussed in the body of this thesis and were shown in Table I, page 15.

A second experiment to measure the relative efficiency of the McKibben counter from thirty kev to one hundred kev was also attempted. For this experiment the pressure of hydrogen in the counter had to be reduced so that the counter would produce pulses well above electrical noise. A hydrogen pressure of ten centimeters of mercury was found to be satisfactory for this energy region. In order to observe the pulse height spectrum in this energy range with minimum experimental difficulty the hydrogen counter was placed at zero degrees with respect to the

proton beam and a spectrum was taken at neutron energies of about thirty and one hundred kev. The center of mass motion of the Li(p,n) reaction just above forward threshold produces a neutron beam at zero degrees of approximately thirty kev energy. A reasonably good pulse height spectrum was produced by thirty or one hundred kev neutrons, but it was not possible to measure the efficiency of the McKibben counter relative to that of the recoil counter at a neutron energy of thirty kev. The neutron beam was unstable because of the rapid change in neutron flux with proton energy and the emission angle of the neutrons. However, the experiment did indicate that the hydrogen counter was capable of measuring the flux of monoenergetic neutron beams in the energy range from 30 to 100 kev, as well as from 100 to at least 650 kev.

A second attempt to measure the flatness of response of the McKibben counter in the energy range of thirty to one hundred kev was made at ninety degrees with respect to the proton beam where a reasonably monoenergetic neutron flux is available. When this procedure was followed, the pulse height spectrum from the hydrogen counter was very poor due to neutrons scattered from the forward angle. Since the background due to scattered neutrons was large compared to the counting rate from the desired monoenergetic neutron beam, a reasonably accurate interpretation of the pulse height spectrum of the recoil counter was not possible. Thus the experiment to measure the relative efficiency of the McKibben counter for neutrons of energy between thirty and one hundred kev was not feasible. The recoil counter was therefore

used as a standard only above a neutron energy of one hundred kev. The $B^{10}(n, \alpha)$ cross section was found to be a satisfactory standard at lower energies (see Chapter I, Monitors).

REFERENCES

REFERENCES

1. B. L. Henkel and H. H. Barshall, Phys. Rev. 80, 145 (1950).
2. G. A. Linenberger and J. A. Miskel, Los Alamos Report 467 (1946).
3. H. Feshbach, C. E. Porter, and V. F. Weisskopf, Phys. Rev. 96, 448 (1954).
4. H. H. Barschall, Phys. Rev. 86, 431 (1952).
5. A. Okazaki, Phys. Rev. 99, 55 (1955).
6. H. Marshak and H. W. Newson, Phys. Rev. 106, 110 (1957).
7. F. Borelli and S. E. Darden, Phys. Rev. 109, 2079 (1958).
8. R. E. Cote, L. M. Bollinger, and J. M. LeBlanc, Phys. Rev. 111, 288 (1958).
9. K. K. Seth, Bull. Am. Phys. Soc. 3, 224 (1958).
10. D. J. Hughes, R. L. Zimmerman, and R. E. Chrien, Phys. Rev. Letters 1, 461 (1958).
11. H. W. Newson, R. C. Block, P. F. Nichols, A. Taylor, and A. K. Furr, Ann. Phys. 8, 211 (1959).
12. K. K. Seth, E. G. Bilpuch, and H. W. Newson, Bull. Am. Phys. Soc. 5, 18 (1960).
13. E. G. Bilpuch, Unpublished Ph.D. thesis, Univ. of North Carolina (1956), 70 pages.
14. A. V. Masket, unpublished.
15. D. J. Hughes and R. B. Schwarz, Neutron Cross Sections (BNL-325) (U.S. Government Printing Office, Washington 25, D.C., 1958), second edition.
16. H. O. Hanson and J. L. McKibben, Phys. Rev. 72, 673 (1947).
17. R. H. Rohrer, unpublished.
18. J. H. Gibbons, Phys. Rev. 102, 1574 (1956).

19. C. T. Hibdon and C. O. Muelhause, unpublished Argonne National Laboratory document (ANL-4552, p. 6).

20. H. W. Schmitt, R. C. Block, and R. L. Bailey, unpublished.

21. J. H. Gibbons, private communication.

22. H. Bichsel and T. W. Bonner, Phys. Rev. 128, 1025 (1957).

23. R. Taschek and A. Hemmendinger, Phys. Rev. 74, 373 (1948).

24. E. R. Rae, B. Margolis, and E. S. Troubetzkoy, Phys. Rev. 112, 492 (1958).

25. J. M. C. Scott, Phil. Mag. 45, 1322 (1954).

26. D. J. Hughes and J. A. Harvey, Phys. Rev. 99, 1032 (1955).

27. C. E. Porter and R. G. Thomas, Phys. Rev. 104, 483 (1956).

28. Table Of The Error Function And Its Devivative, National Bureau of Standards Series 41 (U.S. Government Printing Office, Washington 25, D.C., 1954), first edition, Vol. I.

29. A. M. Lane and J. E. Lynn, Proc. Phys. Soc. 70A, 557 (1957).

30. L. Dresner, Unpublished Ph.D. thesis (O.R.N.L.-2659), (1959).

31. D. J. Hughes, R. C. Garth, and C. Eggler, Phys. Rev. 83, 234 (1951).

32. S. Fernbach, Rev. Mod. Phys. 30, 415 (1958).

33. L. W. Weston, K. K. Seth, E. G. Bilpuch, and H. W. Newson, Ann. Phys., submitted for publication.

34. A. Stolovy and J. A. Harvey, Phys. Rev. 108, 353 (1957).

35. J. M. B. Lang and K. J. Lecouteur, Proc. Phys. Soc. 67A, 586 (1954).

36. H. W. Newson and M. M. Duncan, Phys. Rev. Letters 3, 45 (1959).

37. J. H. Gibbons, P. D. Miller, H. H. Neiler, and R. L. Macklin, private communications.

38. P. A. Moldauer, Bull. Am. Phys. Soc. 4, 475 (1959).

39. A. G. W. Cameron, private communication.

40. K. K. Seth, Can. J. Phys. 37, 1199 (1959).

41. K. K. Seth, Ann. Phys. 8, 223 (1959).

42. K. K. Seth et al., unpublished.

43. A. I. Leipunsky, O. D. Kazachkovsky, G. H. Artyukov, A. I. Baryshnikov, V. I. Galkov, Y. Y. Stavissky, E. A. Stumbur, and L. E. Sherman, Proceedings of the Second International Conference on the Peaceful Uses of Atomic Energy (United Nations Publication, 1958), Vol. 15, p. P/2219.

44. A. E. Johnsrud, M. G. Silbert, and H. H. Barschall, Bull. Am. Phys. Soc. 3, 165 (1958).

45. R. L. Macklin, N. H. Lazar, and W. S. Lyon, Phys. Rev. 107, 504 (1957).

46. J. F. Vervier, Nucl. Phys. 9, 569 (1959).

47. F. G. P. Seidl, D. G. Hughes, H. Palevsky, J. S. Levin, W. Kato, and N. G. Sjöstrand, Phys. Rev. 95, 476 (1954).

48. R. G. Fluharty, F. B. Simpson, and O. D. Simpson, Phys. Rev. 103, 1778 (1956).

49. E. R. Rae, E. R. Collins, B. B. Kinsey, J. E. Lynn, and E. R. Wiblin, Nucl. Phys. 5, 89 (1958).

50. S. Desjardins, Unpublished Ph.D. thesis (CU-189), Columbia University (1959), 111 pages.

51. R. L. Macklin and W. S. Lyon, unpublished A.E.C. document (Report to the Nuclear Cross Sections Advisory Group, 59-2-83, 1958).

52. H. W. Schmitt, C. W. Cook, and J. H. Gibbons, Bull. Am. Phys. Soc. 4, 474 (1959).

53. R. Booth, W. P. Ball, and M. H. MacGregor, Phys. Rev. 112, 226 (1958).

54. B. C. Diven and J. Terrell, private communication.

55. Vladimirskii, Radewich and, Sokolowsky, Proceedings of the International Conference on Peaceful Uses of Atomic Energy (United Nations Publication, 1956), Vol. 4, p. 641.

56. S. Desjardins, J. L. Rosen, J. Rainwater, and W. W. Havens, Jr., Bull. Am. Phys. Soc. 5, 32 (1960).

57. V. Hummel and B. Hamermesh, Phys. Rev. 82, 67 (1951).

58. D. J. Hughes, R. C. Garth, and J. S. Levin, Phys. Rev. 91, 1423 (1953).

59. A. Saplakoglu, L. M. Bollinger, and R. E. Cote, Phys. Rev. 109, 1258 (1958).

60. J. L. Rosen, S. Desjardins, W. W. Havens, Jr., and J. Rainwater, Bull. Am. Phys. Soc. 4, 473 (1959).

61. A. E. Glassgold, Revs. Modern Phys. 30, 419 (1958).

62. H. W. Newson, R. M. Williamson, K. W. Jones, J. H. Gibbons, and H. Marshak, Phys. Rev. 108, 1294 (1957).

63. R. L. Macklin and J. H. Gibbons, Phys. Rev. 109, 105 (1958).

64. J. H. Gibbons and H. W. Newson, Fast Neutron Physics (Interscience Publishers, Inc., New York, 1960), Volume IV, Part I, Section I.E., p. 170.

65. W. D. Allen and A. T. G. Ferguson, unpublished Atomic Energy Research Establishment document (Harwell, England, A.E.R.E. - NP/R 1720, 1955).

66. T. H. R. Skyrme, P. R. Tunnicliffe, and A. G. Ward, Rev. Sci. Instr. 23, 204 (1952).

67. P. K. Weyl, Phys. Rev. 91, 289 (1953).

AUTOBIOGRAPHICAL SKETCH

Date of Birth: November 18, 1932

Place of Birth: Greenwood, Florida

Undergraduate Study: Florida State University
B.S. (Physics), 1954

Graduate Study: Duke University 1954 to Present
Teaching Assistant 1954-1955
Research Assistant 1955-1960
Candidate for Ph.D. Degree, June, 1960

Publications:

1. E. G. Bilpuch, L. W. Weston, and H. W. Newson, "Neutron Capture Cross Sections in the kev Region. Part I: Methods of Measurement and Analysis," submitted for publication in Annals of Physics.

2. L. W. Weston, K. K. Seth, E. G. Bilpuch, and H. W. Newson, "Neutron Capture Cross Sections in the kev Region. Part II: Spin-Orbit Coupling and the Optical Model," submitted for publication in Annals of Physics.

Professional Society: Sigma Xi